HHS Public Access

Author manuscript

J Immunol. Author manuscript; available in PMC 2017 August 15.

Published in final edited form as:

J Immunol. 2016 August 15; 197(4): 1353–1367. doi:10.4049/jimmunol.1600699.

Active caspase-1 induces plasma membrane pores that precede pyroptotic lysis and are blocked by lanthanides[#]

Hana M. Russo[*], **Joseph Rathkey**[*], **Andrea Boyd-Tressler**[&], **Michael A. Katsnelson**[*], **Derek W. Abbott**[*], and **George R. Dubyak**[+,*,&]

[+]Department of Physiology/Biophysics, Case Western Reserve University, Cleveland, OH 44106, USA

[*]Department of Pathology, Case Western Reserve University, Cleveland, OH 44106, USA

[&]Department of Pharmacology, Case Western Reserve University, Cleveland, OH 44106, USA

Abstract

Canonical inflammasome activation induces a caspase-1/gasdermin D (Gsdmd) dependent lytic cell death called pyroptosis which promotes anti-microbial host defense but may contribute to sepsis. The nature of the caspase-1-dependent change in plasma membrane (PM) permeability during pyroptotic progression remains incompletely defined. We assayed propidium^{2+} (Pro^{2+}) influx kinetics during NLRP3 or Pyrin inflammasome activation in murine bone marrow-derived macrophages (BMDM) as an indicator of this PM permeabilization. BMDM were characterized by rapid Pro^{2+} influx after initiation of NLRP3 or Pyrin inflammasomes by nigericin or *C. difficile* toxin B (TcdB), respectively. No Pro^{2+} uptake in response to nigericin or TcdB was observed in *Caspase-1*$^{-/-}$ or *ASC*$^{-/-}$ BMDM. The cytoprotectant glycine profoundly suppressed nigericin and TcdB-induced lysis but not Pro^{2+} influx. The absence of Gsdmd expression resulted in suppression of nigericin-stimulated Pro^{2+} influx and pyroptotic lysis. Extracellular La^{3+} and Gd^{3+} rapidly and reversibly blocked the induced Pro^{2+} influx and markedly delayed pyroptotic lysis without limiting upstream inflammasome assembly and caspase-1 activation. Thus, caspase-1 driven pyroptosis requires induction of initial pre-lytic pores in the PM that are dependent on Gsdmd expression. These PM pores also facilitated the efflux of cytosolic ATP and influx of extracellular Ca^{2+}. Although lanthanides and Gsdmd deletion both suppressed PM pore activity and pyroptotic lysis, robust IL-1β release was observed in lanthanide-treated BMDM but not in Gsdmd-deficient

[#]The study was supported in part by NIH grants R01-GM36387 (G. Dubyak), R01-EY014362 (G. Dubyak), R01-GM086550 (D. Abbott), P01-DK091222 (D. Abbott), National Multiple Sclerosis Society grant NMSS RG5130A2/1 (GRD). Hana M. Russo was supported in part by NIH training grants T32-AI089474 and T32-GM007250. Joseph Rathkey was supported in part by NIH training grant T32-GM007250. Michael A. Katsnelson was supported in part by 13PRE16860052 Predoctoral Fellowship from the American Heart Association and NIH training grants T32-HL105338 and T32-GM007250.

Author Contributions

HMR and GRD conceived and coordinated the study and wrote the paper. HMR performed and analyzed the experiments in Figures 1, 2, 3C–E, 4, 5, 6, 7, and Supplemental Figures 1, 2, and 3. JR and DWA conceived and generated the CRISPR/ Cas9 protocols for generation of the gasdermin-D deficient immortalized bone marrow-derived macrophage lines. JR performed the experiment in Figure 3B. ABT performed the extracellular adenine nucleotide accumulation assays in Figure 2H. MAK performed pilot experiments that identified lanthanides as blockers of the pre-lytic pyroptotic pores. All authors reviewed the results and approved the final version of the manuscript.

Conflict of Interest

The authors declare that they have no conflicts of interest with the contents of this article.

cells. This suggests roles for Gsdmd in both passive IL-1β release secondary to pyroptotic lysis and in non-lytic/non-classical IL-1β export.

Keywords

Caspase-1; Inflammasome; Gasdermin D; Lanthanide; Pyroptosis

Introduction

Caspase-1 and murine caspase-11 (caspase-4/5 in humans) mediate a lytic, inflammatory mode of cell death known as pyroptosis. Active caspase-1 is generated by proximity-induced autocatalytic cleavage of pro-caspase-1 following the assembly and oligomerization of a canonical inflammasome complex which occurs in response to a wide variety of cellular stressors and microbial stimuli. A non-canonical inflammasome involves the direct binding of the lipid A portion of LPS to pro-caspase-11 which facilitates pro-caspase-11 oligomerization and proximity-induced autocatalytic cleavage to form active caspase-11 (1). Caspase-1, but not caspase-11, is also required to process the inflammatory cytokines pro-IL-1β and pro-IL-18 into their mature forms. Depending on myeloid cell type or mode of inflammasome activation, IL-1β may be released passively as a secondary consequence of pyroptotic cell lysis or through incompletely defined non-classical export pathways that are independent of cell lysis (2–5).

Pyroptosis is an effective immune defense mechanism against intracellular bacterial infection. It allows for the removal of intracellular bacteria from their replicative niche and their subsequent detection and efficient clearance by recruited neutrophils (6). However, if the extent of host cell pyroptosis becomes excessive, it can contribute to sepsis and septic shock. Vance and colleagues reported that NLRC4 inflammasome-induced pyroptotic signaling in response to the rapid cytosolic delivery of bacterial flagellin involved Ca^{2+} influx and massive eicosanoid biosynthesis and release which led to enhanced vascular permeability and septic shock in mice (7). Notably, caspase-11-dependent pyroptosis is a critical mediator of LPS-induced lethal sepsis in mice (8–10).

In the context of HIV infection and chronic inflammatory conditions, pyroptosis can also be deleterious to the host. During HIV infection, incomplete DNA transcripts from non-productively infected $CD4^+$ T-cells can be recognized by the IFI16 inflammasome resulting in pyroptosis; this causes massive $CD4^+$ T-cell loss and chronic inflammation (11). Pyroptosis can also promote chronic inflammation by providing a lytic pathway for release of ASC specks which are active inflammasome complexes based on stable polymerized assemblies of the adaptor protein ASC (12). These externalized ASC specks enable continued processing of IL-1β and propagate inflammasome activation following their internalization by bystander phagocytes (12).

Recently, gasdermin D (Gsdmd) was identified as a downstream substrate of caspase-1/11/4/5 that is sufficient to execute pyroptotic cell death (13, 14). Gsdmd is a soluble, cytosolic protein with no apparent transmembrane spanning region. In humans, it is the product of one of four members of the *GSDM* gene family (*GSDMA, GSDMB,*

GSDMC, and GSDMD) (15), while the murine genome includes *Gsdma1–3*, *Gsdmc1–4*, and *Gsdmd. GSDM* and *Gsdm* genes are mostly expressed in skin and intestinal epithelial cells (15); murine *Gsdmd,* in particular, is highly expressed in the small intestine and spleen (15). GSDMD is the only human gasdermin-family protein that has a caspase-1/11/4/5 cleavage site; the cleavage sites in human GSDMD and murine Gsdmd are similar but not identical (13).

Caspase-1/11 cleavage of Gsdmd relieves an autoinhibitory interaction between its N and C-termini, such that the N-terminal fragment can mediate lytic cell death (13). Cleavage of Gsdmd by caspase-1 requires caspase-1 recruitment into active inflammasomes but not full processing of caspase-1 (16); this is consistent with an earlier study demonstrating that partially cleaved caspase-1 efficiently mediates NLRC4 inflammasome-dependent pyroptosis (17). In addition to mediating pyroptotic cell death, Gsdmd is also necessary for maximal IL-1β release (13, 14, 16).

Despite the requirement for Gsdmd in caspase-1/11 dependent pyroptosis, the specific mechanism(s) by which Gsdmd induces lytic cell death is incompletely defined. Following caspase-1/11 activation and Gsdmd cleavage, plasma membrane (PM) integrity becomes compromised leading to a perturbation in ion homeostasis, osmotic swelling and lysis, and the release of various inflammatory mediators (18). DNA fragmentation occurs during pyroptosis but is not required for the execution of pyroptotic cell death (19). Earlier studies by Cookson and colleagues reported the formation of plasma membrane pores with a diameter of 1.1–2.4nm during *Salmonella Typhimurium* dependent caspase-1 activation in macrophages; formation of the pores correlated with osmotic swelling and lysis (19). However, the molecular identity of these caspase-1 induced pyroptotic pore(s) remains unknown.

In this study, we investigated the molecular and pharmacological properties of the caspase-1 dependent pyroptotic pores by utilizing two canonical inflammasome model systems – the bacterial ionophore nigericin (NG) to engage NLRP3 inflammasomes and *C. difficile* toxin B (TcdB) to engage Pyrin inflammasomes – in conjunction with kinetic analysis of propidium^{2+} dye influx as a readout of pore activity. We now report that caspase-1 activation rapidly induces a PM pore that is non-selectively permeable to large organic cations and anions and is activated prior to pyroptotic cell lysis. Induction of this pore is critically dependent on the expression of Gsdmd, while its function as an ion permeable conduit is rapidly and reversibly inhibited by the broadly acting channel inhibitors, La^{3+} and Gd^{3+}. These data suggest that caspase-1 cleavage of Gsdmd licenses its function as either a direct pore-forming protein, a chaperone that facilitates efficient pyroptotic pore insertion in the PM, or as a regulator that gates a PM-resident large pore ion channel. Although lanthanides and Gsdmd deletion both suppressed PM pore activity and pyroptotic lysis, robust IL-1β release was observed in lanthanide-treated BMDM but not in Gsdmd-deficient cells. This may indicate roles for Gsdmd in both passive IL-1β release secondary to pyroptotic lysis and in non-lytic/non-classical IL-1β export.

Materials and Methods

Reagents

Key reagents and their sources were are follows: *Escherichia coli* LPS serotype O1101:B4 (List Biological Laboratories), nigericin (NG; APExBio), *C. difficile* Toxin B (TcdB; List Biological Laboratories), glycine (Fisher), $GdCl_3$ (Sigma-Aldrich), $LaCl_3$ (Fisher), trovafloxacin (Sigma-Aldrich), P2X7R antagonists A10606120 and A438079 (Tocris Bioscience), ruthenium red (Tocris Bioscience), NS8593 (Sigma-Aldrich), zVAD-fmk and zDEVD-fmk (APExBio), disuccinimidyl suberate (DSS; Sigma-Aldrich), anti–caspase-1 (p20) mouse mAb (AG-20B-0042) (Adipogen), anti-GSDMDC1 mouse mAb (A-7), anti-ASC rabbit polyclonal Ab (N-15), anti-β actin goat polyclonal Ab (C-11), and all HRP conjugated secondary Abs (Santa Cruz Biotechnology), murine IL-1β ELISA kit (Biolegend), Fluo-4-AM (Life Technologies), probenecid and trovafloxacin (Sigma-Aldrich), propidium iodide (PI; Life Technologies), YoPro iodide (PI; Life Technologies) ethidium homodimer-2 iodide (EthD-2; Life Technologies), adenosine 5'-(α,β-methylene)-diphosphate (APCP) (Jena Bioscience), phosphoenolpyruvate, lyophilized Firefly luciferase ATP assay mix (FLAAM), Firefly luciferase ATP assay buffer (FLAAB), pyruvate kinase (P-1506), and myokinase (M-3003) (Sigma-Aldrich), lactate dehydrogenase (LDH) cytotoxicity detection kit (Roche). Anti–IL-1β mouse mAb was provided by the Biological Resources Branch, National Cancer Institute, Frederick Cancer Research and Development Center (Frederick, MD).

Murine macrophage models and cell culture

Wild-type (WT) C57BL/6 mice were purchased from Jackson Labs. Mice lacking both caspase-1 and caspase-11 on a C57BL/6 background (*Casp1/11*$^{-/-}$) have been previously described (8, 20, 21). ASC$^{-/-}$ and NLRP3$^{-/-}$ (C57BL/6 background) mice were provided by Eric Pearlman and Amy Hise (Case Western Reserve University). P2X7R$^{-/-}$ mice have been previously described (5). All experiments and procedures involving mice were approved by the Institutional Animal Care and Use Committee of Case Western Reserve University. Bone marrow–derived macrophages (BMDM) were isolated from 9- to 12-wk-old mice euthanized by CO_2 inhalation. Femurs and tibiae were removed and briefly immersed in 70% ethanol. Bones were then flushed with PBS to remove marrow cavity plugs. Bone marrow cells were resuspended in DMEM (Sigma-Aldrich) supplemented with 10% bovine calf serum (HyClone Laboratories), 100 U/mL penicillin, 100 μg/mL streptomycin (Invitrogen), 2 mM L-glutamine (Lonza), and 30% L-cell conditioned medium (which contains the M-CSF necessary for BMDM differentiation), and then plated on 150 mm dishes and cultured in the presence of 10% CO_2. Day 3 post-isolation, 80% of medium containing non-adherent cells was centrifuged at 300 x *g* for 5 min and resuspended and replated with fresh BMDM media. Day 5 post-isolation, BMDM were re-fed, and on day 6, BMDM were detached with PBS containing 10mM EDTA and 4mg/mL lidocaine, replated on 6-well, 12-well, or 24-well plates at 1 x 10^6 cells/mL, and used within 4 days.

NLRP3-FLAG overexpressing, ASC-mCerulean immortalized NLRP3 KO murine macrophages (iBMDM) were provided by Eicke Latz (University of Bonn, Bonn, Germany). iBMDM were cultured in DMEM (Sigma-Aldrich) supplemented with 10% heat inactivated

bovine calf serum (HyClone Laboratories), 100 U/mL penicillin, 100 μg/mL streptomycin (Invitrogen), and 2 mM L-glutamine (Lonza). iBMDM were plated on 6-well or 24-well plates at 1 x 10^6 cells/mL, and used within 2 days.

Generation of CRISPR GSDMD$^{-/-}$ iBMDM

A CRISPR-Cas9 guide against *Gsdmd* was inserted into the lentiCRISPRv2 plasmid (22, 23) with puromycin resistance protein replaced with a hygromycin resistance cassette (Chirieleson *et al.* in preparation). CRISPR Oligonucleotides: Gsdmd guide 1-F 5'-CACCGCAGAGGCGATCTCATTCCGG-3', Gsdmd guide 1-R 5'-AAACCCGGAATGAGATCGCCTCTGC -3', Gsdmd guide 2-F 5'-CACCGTGAAGCTGGTGGAGTTCCGC-3', Gsdmd guide 2-R 5'-AAACGCGGAACTCCACCAGCTTCAC-3'. Plasmid lentiCRISPRv2 containing each guide were co-transfected into 293T cells with packaging plasmids PsPax and PMD2. iBMDM were transduced with virus for 2 days and selected with hygromycin. Clonal cells were isolated and loss of Gsdmd verified by western blot.

Priming and stimulation of BMDM and iBMDM

BMDM and iBMDM were primed with 1 μg/ml LPS for 3–4 h at 37°C. LPS containing media was then replaced with a Ca^{2+}-containing balanced salt solution (BSS) (130 mM NaCl, 4 mM KCl, 1.5 mM $CaCl_2$, 1 mM $MgCl_2$, 25 mM Na HEPES, 5 mM D-glucose [pH 7.4]). BSS contained 0.1% bovine serum albumin (BSA) for all assays except for western blot sample preparation, which contained 0.01% BSA. BMDM and iBMDM were stimulated with 10μM NG or 0.4μg/mL TcdB for varying lengths of time as indicated. For lanthanide inhibition studies, BMDM and iBMDM were treated with indicated concentrations of La^{3+} or Gd^{3+} upon stimulation with NG or 20 min after stimulation with TcdB, which is after the toxin has been internalized but prior to pyroptotic pore opening.

Western blot analyses and ASC oligomerization assay

LPS-primed BMDM and iBMDM in 6-well plates (2 x 10^6 cells/well) were treated as indicated in the presence of BSS containing 0.01% BSA. Following 30 min NG stimulation or 45 min TcdB stimulation, detergent-soluble cell lysates and extracellular medium (ECM) fractions were prepared as previously described (24) for standard processing by SDS-PAGE, transfer to PVDF membrane, and Western blot analysis. Briefly, to prepare the detergent-soluble cell lysate, 56uL of RIPA lysis buffer (0.5% sodium deoxycholate, 0.1% SDS, 1% IgePal CA630 in PBS, pH 7.4, plus protease inhibitor mixture) was added to adherent cells on the 6-well plate and incubated on ice for 5 min. Lysed adherent cells were scraped with a rubber policeman and incubated on ice for 15 min. The whole cell lysate was centrifuged at 15,000 x *g* for 15 min at 4°C to separate the detergent-soluble from insoluble fraction. ASC oligomeric complexes were detected in the insoluble fraction as described previously (24). Primary antibodies were used at the following concentrations: 5μg/mL for IL-1β; 1μg/mL for caspase-1; 0.4μg/mL for ASC; 0.2μg/mL for β-Actin; 0.4μg/mL for GSDMD, and HRP-conjugated secondary Abs were used at a final concentration of 0.13μg/mL. Chemiluminescent images of Western blots were developed using a FluorChemE processor (Cell Biosciences).

Propidium^{2+}, YoPro^{2+}, EthD^{4+} influx assays of pyroptotic plasma membrane permeabilization

LPS-primed or non-primed (as indicated) BMDM and iBMDM in 24-well plates (5 x 10^5 cells/well) were briefly washed with PBS prior to adding BSS supplemented either with 1μg/mL propidium^{2+}, 2μM EthD^{4+}, or 1μM YoPro^{2+} to each well. Baseline fluorescence (540 nm excitation–> 620 nm emission for propidium^{2+} or EthD^{4+}; 485 nm excitation–> 540 nm emission for YoPro^{2+} at 30 s intervals) was first recorded with a Synergy HT plate reader (BioTek) preheated to 37°C for 5 min. Cells were routinely stimulated with 10μM NG or 0.4μg/mL TcdB in the presence or absence of 5mM glycine for 45 or 60 min, respectively, and the changes in fluorescence were recorded every 30 s. In some experiments with GsdmD-deficient iBMDM, the nigericin stimulation was extended to 2 or 3 h; where indicated, some wells were supplemented with 50 μM zVAD-fmk, 50 μM zDEVD-fmk, or 30μM trovafloxacin. Dye uptake assays were terminated by permeabilizing the PM with digitonin (50μg/mL) to quantify maximum fluorescence. Fluorescence was expressed as a percentage of maximum fluorescence measured in digitonin-permeabilized cells after subtraction of basal intrinsic fluorescence.

For certain propidium^{2+} assays, BMDM or iBMDM were treated with indicated concentrations of La^{3+} or Gd^{3+} in the presence or absence of 5mM glycine. To address whether lanthanides reversibly inhibit the pyroptotic pore, wells containing propidium^{2+}, NG, and La^{3+}/Gd^{3+} were briefly washed with PBS (to remove the lanthanides) 15 min post-NG stimulation and replaced with fresh BSS containing 1μg/mL of propidium^{2+}. To further investigate the mechanism of lanthanide inhibition of pyroptotic pores, La^{3+}/Gd^{3+} and propidium^{2+} were added at different times during NLRP3 or Pyrin inflammasome signaling, which include the following experimental setups: 1) propidium^{2+} added at the same time as NG/TcdB and La^{3+}/Gd^{3+} added at the same time as NG or 20 min post-TcdB, 2) propidium^{2+} added at the same time as NG/TcdB and La^{3+}/Gd^{3+} added 20 min post-NG or 30 min post-TcdB, or 3) La^{3+}/Gd^{3+} added 20 min post-NG or 30 min post-TcdB and propidium^{2+} added 5 min post-La^{3+}/Gd^{3+} addition.

Cytotoxicity assay (LDH release)

LPS-primed BMDM and iBMDM in 24-well plates (5 x 10^5 cells/well) were treated as indicated at 37°C. Supernatants were removed and centrifuged at 15,000 x *g* for 15 s to pellet detached cells. Cell-free supernatants were assayed for LDH activity (Roche Applied Science) according to the manufacturer's protocol. The released LDH was expressed as a percentage of total LDH content following 2% Triton X-100 induced permeabilization of unstimulated LPS-primed cells.

Fluo-4 assay of cytosolic [Ca^{2+}]

LPS-primed BMDM in 24-well plates (5 × 10^5 cells/well) were loaded with fluo-4-AM and assayed for NG or TcdB-induced changes in cytosolic [Ca^{2+}] as described previously (25) using the Synergy HT reader preheated to 37°C. The changes in fluo-4 fluorescence were used to calculate cytosolic [Ca^{2+}] by standard calibration methods (26).

Measurement of released adenine nucleotides

LPS-primed BMDM in 12-well plates (1 x 10^6 cells/well) were stimulated with 10μM NG in the presence of the CD73 inhibitor APCP (50μM) (to prevent the metabolism of AMP to adenosine) and in the presence or absence of 5mM glycine at 37°C. At the indicated times, supernatants were removed and centrifuged at 12,200 x *g* for 15 s to pellet cells. Cell-free supernatants were assayed for total adenine nucleotide content (ATP+ADP+AMP) as described previously (27).

Data processing and analysis

All experiments were repeated 2–8 times with separate BMDM preparations. Figures illustrating Western blot results are from representative experiments. Figures illustrating quantified changes in pyroptotic propidium^{2+} influx, extracellular LDH activity, cytosolic [Ca^{2+}], or extracellular [adenine nucleotide] represent the means (±SE) from 1–6 independent experiments. Quantified data were statistically evaluated by one-way ANOVA with a Bonferroni post-test using Prism 6.0 software.

Results

A rapidly induced propidium influx is triggered downstream of inflammasome activation but upstream of pyroptotic cell lysis

Previous studies have assayed the uptake of cationic DNA-intercalating fluorescent dyes following the activation of a canonical inflammasome complex as an indicator of caspase-1-induced plasma membrane (PM) permeabilization or pyroptosis (19, 28, 29). Normally, these dyes are impermeant to an intact PM. However, upon perturbation of normal PM barrier function, these dyes can access the nucleus, intercalate with DNA, and fluoresce. PM permeabilization can occur through 1) frank lysis, 2) the gating of resident large pore channels, or 3) the insertion of large protein pores that can accommodate the molecular dimensions of these dyes. Case *et al.* previously used a real-time, kinetic assay of propidium^{2+} (MW: 415 Da) influx to track the progression of pyroptosis in *Legionella*-infected macrophages (29). We adapted a similar protocol to investigate the nature and kinetics of caspase-1-induced PM permeabilization during NLRP3 and Pyrin inflammasome activation in murine bone marrow-derived macrophages (BMDM).

To activate the NLRP3 inflammasome, BMDM were stimulated with the bacterial ionophore nigericin (NG), which functions as a K^+/H^+ exchanger following insertion in the PM and organellar membranes. Insertion of NG into the PM results in a decrease in cytosolic [K^+] which is a necessary signal for NLRP3 inflammasome complex assembly (30, 31). We previously reported that after an ~12 min delay, NG-stimulated murine bone marrow-derived dendritic cells (BMDC) exhibit robust and rapid caspase-1 dependent propidium^{2+} influx (25). WT BMDM stimulated with NG displayed similarly rapid propidium^{2+} influx following a 10–12 min delay with ~60% of the BMDM accumulating dye by 45 min (Fig. 1A). Propidium^{2+} influx was absent in *Nlrp3*$^{-/-}$, *Asc*$^{-/-}$, and *Casp1*$^{-/-}$ (also deficient in caspase-11) BMDM (Fig. 1A), demonstrating that propidium^{2+} uptake is dependent on NLRP3 inflammasome components and caspase-1 activation.

To address whether this caspase-1 dependent PM permeability pathway is conserved among canonical inflammasome platforms, we also utilized a Pyrin inflammasome model. To activate the Pyrin inflammasome, BMDM were stimulated with *C. difficile* toxin B (TcdB). TcdB is one of the main virulence factors involved in the pathogenesis of a *C. difficile* bacterial infection (32, 33), a major cause of hospital-acquired, antibiotic-associated infectious diarrhea and pseudomembranous colitis (34, 35). TcdB-induced Pyrin inflammasome activation requires effective internalization of the toxin into the cytosol followed by TcdB-dependent glycosylation and inactivation of Rho-GTPases (36). Following an ~20 min delay, WT BMDM stimulated with TcdB exhibited rapid and robust propidium^{2+} influx with ~40% of the cells accumulating dye by 60 min (Fig. 1B). Propidium^{2+} influx was almost completely suppressed in *Asc*$^{-/-}$ and *Casp1*$^{-/-}$ BMDM throughout the 60 min TcdB stimulation, but remained intact in *NLRP3*$^{-/-}$ BMDM (Fig. 1B); this demonstrates that TcdB-induced propidium^{2+} uptake is dependent on Pyrin inflammasome components.

We next determined whether caspase-1 induced PM permeabilization indicates a pre-lytic event, like pore/channel opening, or cell lysis. Early studies by Cookson and colleagues found that the cytoprotectant glycine protected *Salmonella*-infected macrophages from end-stage lysis but did not suppress uptake of ethidium^{+}, a smaller (314 Da) DNA-intercalating dye (19, 37, 38). We have also reported the use of glycine to suppress caspase-1-induced lysis of macrophages stimulated with maitotoxin (39) or extracellular ATP (40). Notably, millimolar concentrations of glycine have also been used to characterize maitotoxin and palytoxin-induced changes in PM permeability of endothelial cells (41, 42), as well as the pyroptotic responses in macrophages (19). In all of these models of regulated cell death, glycine was shown to prevent or greatly delay end-stage lysis (19, 41, 42).

We adapted these protocols to dissociate lytic from non-lytic propidium uptake by BMDM in response to NLRP3 and Pyrin inflammasome activation. Stimulation of WT BMDM with NG or TcdB in the presence of 5mM glycine prevented the lytic release of the large macromolecule lactate dehydrogenase (LDH) (140kDa) (Fig. 1C,D), but permitted the influx of propidium^{2+} with a similar kinetic as in the absence of glycine (Fig. 1E, F). This temporal dissociation between the uptake of propidium^{2+} and the release of LDH in the presence of glycine indicates that propidium^{2+} influx reflects an event before cell lysis, such as the insertion or opening of a “pyroptotic pore”.

NLRP3 and Pyrin inflammasome activation licenses the opening of a large, non-selective cation and anion permeable pyroptotic pore

We next characterized the permeability properties of this putative pyroptotic pore. Previous studies by Cookson and colleagues on pyroptosis in *Salmonella*-infected macrophages indicated the accumulation of 1.1–2.4 nm diameter pores that facilitated the influx of molecules in the 500–1450 Da mass range (19). A range of DNA-intercalating cationic dyes with different masses, charges, and shapes can be employed to probe the dimensions of pyroptotic pores (Supplementary Table 1). To define the pores induced by NLRP3 or Pyrin inflammasomes, we assessed permeability to the larger and more highly charged ethidium homodimer-2 dye (EthD^{4+}; MW: 785 Da). After an ~10–12 min delay, WT BMDM

stimulated with NG exhibited a rapid and robust $EthD^{4+}$ influx that was absent in *Casp1*$^{-/-}$ BMDM; this was similar to the WT BMDM $propidium^{2+}$ influx response, albeit with a slower rate of dye uptake (Fig. 2A). WT BMDM stimulated with TcdB also exhibited rapid and robust $EthD^{4+}$ influx after an ~20 min delay similar to the $propidium^{2+}$ influx profile (Fig. 2B).

We verified that the inflammasome-induced permeability to $EthD^{4+}$ was also a pre-lytic event by assessing $EthD^{4+}$ permeability in the presence of glycine. Following the stimulation of WT BMDM with NG or TcdB, the $EthD^{4+}$ uptake profiles were similar in the presence and absence of glycine (Fig. 2C,D); this indicated that the induced pyroptotic pore is permeable to the larger $EthD^{4+}$ dye and thus accommodates large organic molecules in the 800 Da mass range. In contrast, Fink and Cookson observed that $EthD^{4+}$ did not permeate the pyroptotic pore induced in *Salmonella*-infected macrophages (19). This discrepancy might indicate that pores of varying dimensions can accumulate during pyroptotic induction by different inflammasome subtypes or that pyroptotic pore induction and its dimensions vary dynamically depending on the rate and extent of active caspase-1 accumulation. Indeed, Gaidt *et al.* (4) recently reported that stimulation of human monocytes with LPS alone induced distinct NLRP3-dependent inflammasomes that did not drive pyroptotic lysis, while stimulation of the same monocytes with LPS plus nigericin resulted in robust NLRP3 inflammasome-dependent pyroptosis.

Given the pyroptotic pore's permeability to large organic cations, we next characterized its ability to act as a conduit for inorganic cations or organic anions. To assess the permeability of the pore to Ca^{2+}, fluo-4 Ca^{2+} indicator dye was loaded into BMDM prior to acute induction of NLRP3 or Pyrin inflammasomes. WT BMDM stimulated with NG exhibited a modest and gradual rise in cytosolic [Ca^{2+}] after a 10–12 min delay and this response was absent in *Casp1*$^{-/-}$ BMDM (Fig. 2E). We previously reported similar caspase-1 dependent increases in cytosolic [Ca^{2+}] in NG-stimulated BMDC and demonstrated that this involved influx of extracellular Ca^{2+} rather than mobilization of intracellular Ca^{2+} stores (25). WT BMDM stimulated with TcdB also demonstrated a gradual rise in cytosolic [Ca^{2+}] concentration after an ~ 20 min delay that was greatly suppressed in *Casp1*$^{-/-}$ BMDM (Fig. 2F). The onset of Ca^{2+} influx temporally correlated with the onset of $propidium^{2+}$ influx in both inflammasome models; this suggests that the rise in cytosolic [Ca^{2+}] is predominantly mediated by the induced pyroptotic pore. That the Ca^{2+} influx profiles of WT BMDM in response to NG or TcdB were similar in the presence and absence of glycine (Fig. 2G) indicates that Ca^{2+} influx, like $propidium^{2+}$ and $EthD^{4+}$ uptake, reflects a pre-lytic change in PM permeability.

To assess if the pyroptotic pore is also permeable to anions, particularly intracellular metabolites such as ATP, the extracellular medium from WT and *Casp1*$^{-/-}$ BMDM stimulated with NG was assayed for total adenine nucleotide (ATP+ADP+AMP) content. The collected samples were treated with a cocktail of myokinase, pyruvate kinase, and phosphoenolpyruvate to convert extracellular AMP and ADP to ATP and a luciferase-based assay was used to determine [ATP]. We were particularly interested in whether the pyroptotic pore is permeable to ATP because this nucleotide is an important danger-associated molecular pattern (DAMP) that activates innate immune cells for support of

adaptive immune responses (43, 44) and also promotes leukocyte chemotaxis (45). In the absence or presence of glycine, NG-stimulated WT BMDM progressively released comparable amounts of adenine nucleotides after an ~10 min delay, and this release was absent in *Casp1*$^{-/-}$ BMDM (Fig. 2H). This indicates that adenine nucleotides are released through a caspase-1 induced pore rather than as a secondary consequence of cell lysis. Taken together, these results indicate that caspase-1 activation induces a large non-selective cation- and anion-permeable pore in the macrophage PM that precedes overt cell lysis.

Gasdermin D is required for caspase-1 induction of both the pre-lytic pyroptotic pores and subsequent pyroptotic lysis

Because gasdermin D (Gsdmd) was recently identified as a downstream target of caspase-1/11 with the resulting N-terminal cleavage product being necessary to execute pyroptotic cell death (13, 14, 16), we hypothesized that Gsdmd was also required to induce the pyroptotic pore/channel. He *et al.* (16) used end-point fluorescence imaging to demonstrate nigericin-stimulated propidium^{2+} staining in control but not Gsdmd-deficient murine macrophages. However, those single time point images at 60 min did not distinguish between pre-lytic versus post-lytic dye accumulation. We utilized *Gsdmd*-targeting guide RNAs (gRNAs) and immortalized murine bone marrow-derived macrophages (iBMDM) to generate CRISPR-Cas9 *Gsdmd*$^{-/-}$ iBMDM cell lines (Fig. 3A). Pooled iBMDM clones generated with two separate gRNA (*Gsdmd* G1 and *Gsdmd* G2) lacked immunoreactive Gsdmd protein and were used for subsequent experiments (Fig. 3B). In response to NG stimulation, LPS-primed *Gsdmd*$^{-/-\,G1}$ and *Gsdmd*$^{-/-\,G2}$ iBMDM exhibited no propidium^{2+} uptake at early time points, whereas the parental WT iBMDM and WT iBMDM transduced with a non-targeting gRNA (NTG) displayed robust propidium^{2+} uptake that was markedly suppressed by the pan-caspase inhibitor zVAD (Fig. 3C). As expected, Gsdmd was also necessary for downstream lysis because *Gsdmd*$^{-/-\,G1}$ and *Gsdmd*$^{-/-\,G2}$ iBMDM exhibited complete suppression of LDH release following 30 or 60 min of NG stimulation (Fig. 3D); such blockade of pyroptosis is consistent with previous findings (13, 16). We also verified that glycine retards the lytic release of LDH 30 min post-NG stimulation in WT iBMDM similarly to its effect on WT primary BMDM (Supplemental Fig. 1A). These data demonstrate that Gsdmd is required to induce the upstream pre-lytic pyroptotic pore/channel that mediates propidium^{2+} influx and eventually leads to end-stage pyroptotic cell lysis.

During prolonged NLRP3 inflammasome activation in the absence of Gsdmd, macrophages eventually divert to apoptosis (16). Apoptotic caspase-7 is a substrate of caspase-1 (46) and, in the absence of Gsdmd, macrophages accumulated cleaved caspase-3/7 and active caspase-8 within several hours after assembly of caspase-1 inflammasomes. He et al. (16) also reported that Gsdmd-null macrophages accumulated nuclear propidium^{2+} after 3h of nigericin stimulation. The dye accumulation in the Gsdmd-defiecient cells may reflect lytic uptake due to secondary necrosis and/or pre-lytic influx through other large pore ion channels, such as pannexin-1. Nunez and colleagues recently described an alternative pyroptotic pathway initiated by caspase-11-dependent cleavage of pannexin-1 channels in murine macrophages (47). We used nigericin-stimulated Gsdmd-deficient iBMDM to define alternative modes by which accumulation of active caspase-1 can alter PM permeability. After an ~60 min delay, the cells began to accumulate propidium^{2+} and this response was

completely suppressed by the pan-caspase inhibitor zVAD or caspase-3-selective inhibitor DEVD, but not the pannexin-1 blocker trovafloxacin (Fig. 3E). Activated pannexin-1 channels have low permeability to propidium^{2+} but high permeability to YoPro^{2+} which has the same charge but smaller mass (375 Da) compared to propidium^{2+} (Supplemental Table 1) (27, 48–50). In response to nigericin, Gsdmd-null iBMDM displayed a delayed and zVAD-sensitive increase in YoPro^{2+} accumulation (Fig. 3E). Notably, trovafloxacin produced a two-fold decrease in the rate of YoPro^{2+} uptake. This suggests that caspase-3/7-gated pannexin-1 channels contribute to the altered PM permeability of inflammasome-activated macrophages under conditions of suppressed pyroptosis.

Lanthanides coordinately suppress both the caspase-1-dependent plasma membrane permeability change and pyroptotic lysis induced by NLRP3 and Pyrin inflammasome activation

To further characterize the molecular and biophysical properties of the caspase-1-Gsdmd-induced pore and its mechanistic coupling to pyroptotic cell death, we investigated whether the pore could be targeted pharmacologically. Given its non-selective permeability to large organic and inorganic cations and anions, we tested whether activity of the pyroptotic pore might be blocked by lanthanides (Gd^{3+} and La^{3+}) which are broadly acting channel inhibitors. Lanthanides are known to inhibit non-selective cation channels (51) and a broad range of large-pore channels (52). WT BMDM stimulated with NG in the presence of 1mM Gd^{3+} or La^{3+} were characterized by modest decreases in the rate of propidium^{2+} influx relative to that observed in lanthanide-free medium (Fig. 4A,B). The rate and magnitude of suppression was much greater as the lanthanide concentration increased to 1.2mM (Gd^{3+}: ~60% mean suppression, La^{3+}: 100%) and 1.5mM (Gd^{3+}: ~90% mean suppression, La^{3+}: 100%) (Fig. 4A,B). Thus, the inhibitory effects of lanthanides on pyroptosis-induced PM permeabilization were defined by very steep concentration-response relationships with La^{3+} as a modestly more potent suppressor compared to Gd^{3+}. We verified that the lanthanides similarly suppressed the pyroptotic PM permeability change induced by pyrin inflammasomes. In these experiments, the BMDM were treated with increasing concentrations of Gd^{3+} or La^{3+} added 20 min post-TcdB, which is after the toxin has been internalized but prior to initiation of propidium^{2+} influx. 1mM Gd^{3+} or La^{3+} induced a marked suppression in the rate and magnitude of propidium^{2+} influx (Gd^{3+}: ~30% mean suppression, La^{3+}: ~60% mean suppression) (Fig. 4C,D). The efficacy of blockade was increased as the concentrations were increased to 1.2mM (Gd^{3+}: ~60% mean suppression, La^{3+}: ~70% mean suppression) and 1.5mM (Gd^{3+}: ~90% mean suppression, La^{3+}: ~90% mean suppression) (Fig. 4C,D). These results demonstrate that the lanthanides suppress pyroptotic propidium^{2+} influx downstream of two distinct inflammasome signaling pathways.

We next determined whether the lanthanides also suppress the downstream execution of pyroptotic cell death by assaying LDH release as an indicator of lysis. WT BMDM stimulated with NG for 30 min (a time point corresponding to active pyroptotic propidium^{2+} influx) in the presence of 1.2mM Gd^{3+} or La^{3+} released markedly less LDH compared to cells stimulated with NG in lanthanide-free medium (Fig 4E). In the presence of 1.2mM Gd^{3+} or La^{3+}, the percent suppression of LDH release (Gd^{3+}: 67% mean suppression, La^{3+}:

86% mean suppression) was comparable to the percent suppression of NG-induced propidium^{2+} influx (Gd^{3+}: 70% mean suppression, La^{3+}: 99% mean suppression) over 30 min test periods (Fig. 4E,G). Pyroptotic cell death induced by TcdB-stimulated pyrin inflammasome activation was similarly attenuated by the lanthanides (Fig. 4F,H). In the presence of 1mM Gd^{3+} or La^{3+}, the percent suppression of LDH release (Gd^{3+}: 48% mean suppression, La^{3+}: 58% mean suppression) was comparable to the percent suppression of propidium^{2+} influx (Gd^{3+}: 45% mean suppression, La^{3+}: 71% mean suppression) (Fig. 4F,H). Taken together these data demonstrate that – similar to the phenotype of Gsdmd-deficient macrophages – inflammasome-activated WT BMDM are characterized by a profound suppression in both caspase-1-mediated PM permeabilization and downstream pyroptotic cell lysis in the presence of lanthanides.

Lanthanides have previously been used to probe inflammatory signaling responses in other inflammasome models. Yang *et al.* (47) found that Gd^{3+} did not suppress LDH release in their model of caspase-11/pannexin-1-mediated pyroptosis. However, that study tested only 100 μM Gd^{3+}, a concentration that was also submaximal for blocking propidium^{2+} influx and LDH release in our model of caspase-1/Gsdmd-mediated pyroptosis (Supplemental Figs. 1 and 3). Compan *et al.* (53) used 2 mM Gd^{3+} or 2 mM La^{3+} to block IL-1β release and YoPro^{2+} uptake in response to hypotonicity-stimulated NLRP3 inflammasome activation. In that model, the lanthanides were employed to block activity of the TRPM7 and TRPV2 ion channels which functioned as upstream regulators of the volume-sensitive caspase-1 activation response. This contrasts with our use of the lanthanides to block downstream responses to caspase-1 activation by canonical inflammasome stimuli. Lee *et al.* (54) employed 1 mM extracellular Gd^{3+} as an agonist for the G protein-coupled calcium-sensing receptor (CaSR) that was linked to NLRP3 inflammasome activation. In contrast, we observed no stimulatory effects of the lanthanides per se on pyroptotic signaling or inflammasome activation when added alone in the absence of nigericin (data not shown). A caveat in interpretation of the Lee *et al.* finding is that the Gd^{3+} was added to phosphate-containing medium which can result in formation of insoluble gadolinium phosphate particles, phagocytosis of the particles, and subsequent lysosome destabilization, a known NLRP3 activation stimulus (31).

Interestingly, there was an escape from lanthanide suppression of lytic LDH release as the duration of NLRP3 or pyrin inflammasome stimulation was prolonged (Supplemental Fig. 2A–C). Also, there was a more rapid escape from pyroptotic suppression in the presence of 1mM versus 1.2mM concentrations of Gd^{3+} or La^{3+} during NG stimulation (Supplemental Fig. 2A, B). This suggests either a time-dependent loss in efficacy of lanthanide suppression and/or that signaling events downstream of caspase-1/Gsdmd target the integrity of intracellular organelle compartments, as well as the PM to facilitate the execution of pyroptotic cell death.

In contrast to the escape from lanthanide suppression of LDH release with longer duration (60 min) NG stimulation in WT BMDM (Supplemental Fig. 2A, B), *Gsdmd*$^{-/-\,C1}$ and *Gsdmd*$^{-/-\,C2}$ iBMDM maintained complete suppression of LDH release at 60 min post-NG stimulation (Fig. 3D). Sustained suppression of lytic death in the absence of Gsdmd further

suggests that, in addition to PM pyroptotic pore induction, Gsdmd may target other intracellular signaling responses that contribute to the pyroptotic cell death process.

We verified that lanthanides attenuate caspase-1 dependent pyroptotic signaling in iBMDM similarly to their actions in primary BMDM. As in primary WT BMDM, concentrations of Gd^{3+} or La^{3+} greater than 1mM markedly attenuated propidium^{2+} influx in WT iBMDM in response to NG (Supplemental Fig. 1B, C). Likewise, 1.2mM Gd^{3+} or La^{3+} suppressed downstream lytic LDH release at 30 min post-NG stimulation in WT iBMDM (Supplemental Fig. 1D). However, at 60 min following NG stimulation, WT iBMDM exhibited an escape from lanthanide-suppression of LDH release similarly to primary WT BMDM (Supplemental Fig. 1D).

Lanthanides do not block NLRP3 inflammasome activation or IL-1β release while Gsdmd deficiency also does not block NLRP3 inflammasome activation but does block IL-1β release

To test whether the lanthanides might suppress downstream pyroptotic signaling by inhibiting upstream inflammasome assembly or activity, we assayed various indices of inflammasome activation in response to NG (Fig. 5) or TcdB (Supplemental Fig. 2D) stimulation in the presence of Gd^{3+} or La^{3+}. Following 30 min of NG stimulation in the presence of 1, 1.2, 1.5mM Gd^{3+} or La^{3+} (concentrations that suppress pyroptotic propidium^{2+} influx in a dose-dependent manner), WT BMDM displayed intact ASC oligomerization (Fig. 5A), suggesting the assembly of an ASC-containing inflammasome complex. Control experiments (data not shown) indicated that treatment the BMDM with lanthanides alone produced no stimulatory or inhibitory effects on ASC oligomerization, caspase-1 activation, or IL-1β release.

Increasing concentrations of Gd^{3+} or La^{3+} resulted in an enhanced retention of processed caspase-1 in the cell lysate during 30 min incubations with NG (Fig. 5A). The production of processed caspase-1 in the presence of Gd^{3+} and La^{3+} further demonstrated that the lanthanides do not limit NLRP3 inflammasome complex assembly and downstream caspase-1 activation. Notably, at the 1, 1.2, and 1.5mM concentrations of Gd^{3+} or La^{3+}, pro-caspase-1 was predominantly retained in the cell lysate, whereas in the absence of Gd^{3+} and La^{3+} (or at the 300 μM concentration that does not suppress pyroptosis), some pro-caspase-1 was released into the extracellular medium (ECM) (Fig. 5A).

We also examined the effect of lanthanide treatment on the extent of mature IL-1β production as an additional index of inflammasome activation. Western blot analysis revealed that WT BMDM, stimulated with NG for 30 min in the presence of concentrations (>1 mM) of Gd^{3+} and La^{3+} that inhibit pyroptotic dye uptake, generated and released mature IL-1β in amounts comparable to that observed in the absence of lanthanides (Fig. 5A). This marked production of mature IL-1β in the presence of Gd^{3+} and La^{3+} further demonstrates that the lanthanides do not limit NLRP3 inflammasome activation. Importantly, the additional presence of glycine to attenuate cell lysis did not modulate the effects of the lanthanides on nigericin-stimulated NLRP3 inflammasome signaling and IL-1β export (Fig. 5b).

The inhibitory effects of lanthanides on pyroptotic signaling responses downstream of inflammasome activation mostly mimicked the effects of Gsdmd knockout with the following notable exception: release of caspase-1 processed mature IL-1β to the extracellular compartment. We confirmed previous findings (16) that Gsdmd-deficiency does not limit upstream inflammasome activation in response to NG. WT, *Gsdmd*$^{-/-\,G1}$, and *Gsdmd*$^{-/-\,G2}$ iBMDM were stimulated with NG for 30 min, and the formation of mature caspase-1 and IL-1β and the oligomerization of ASC were assayed by western blot. The cell lysates of unstimulated WT iBMDM, but not the *Gsdmd*$^{-/-}$ cells, contained full-length 53 kDa Gsdmd that was extensively processed to the 31kDa N-terminal fragment following NG stimulation; this is consistent with previous reports that active caspase-1 cleaves Gsdmd to produce a 31kDa N-terminal pro-pyroptotic product (13, 14, 16). Both WT and *Gsdmd*$^{-/-}$ iBMDM exhibited intact ASC oligomerization and robust accumulation of processed caspase-1 and IL-1β (Fig. 5C), indicating that Gsdmd mediates downstream pyroptosis but not upstream NLRP3 inflammasome activation.

Notably, mature IL-1β and caspase-1 were completely retained in the cell lysates of the *Gsdmd*$^{-/-}$ iBMDM but were predominantly released into the extracellular medium (ECM) fraction of WT iBMDM (Fig. 5C). Non-lytic IL-1β and caspase-1 release represented a major mode of export because comparable amounts of mature IL-1β and caspase-1 were present in the ECM fractions of WT iBMDM in the presence or absence of glycine (Fig. 5C). Therefore, the absence of Gsdmd does not simply prevent release of caspase-1 and IL-1β as a consequence of blocked pyroptotic lysis, but also suppresses the non-lytic export of these cytosolic proteins that has been previously described in multiple models of inflammasome function (2, 3).

Whereas NG-stimulated *Gsdmd*$^{-/-}$ macrophages were characterized by intracellular retention of both mature IL-1β and the p20 subunit of active capase-1 (Fig. 5C), WT BMDM treated with NG in the presence of lanthanides retained the active p20 caspase-1 in the cytosol but released mature IL-1β to the ECM. To clarify how the absence of Gsdmd, but not the presence of lanthanides, completely suppressed the release of IL-1β, we further investigated the effect of lanthanide treatment on caspase-1 and IL-1β export. Interestingly, concentrations of Gd^{3+} and La^{3+} that inhibit caspase-1-induced PM permeabilization (1, 1.2, 1.5mM) also greatly suppressed caspase-1 release but permitted robust IL-1β release in response to 30 min of NG stimulation (Fig. 5A). Also, similar amounts of 20kDa caspase-1 and mature IL-1β were present in the ECM fraction in the presence and absence of the cytoprotectant glycine, which prevents cell lysis (Fig. 5A, B). These data suggest that Gsdmd knockout per se and lanthanide blockade of the Gsdmd-dependent PM permeability change regulate non-lytic caspase-1 and IL-1β export in distinct ways. Lanthanide inhibition of Gsdmd-induced PM permeabilization markedly limits non-lytic caspase-1 release; however, it permits robust IL-1β release which further underscores an apparent role for Gsdmd in the non-lytic vesicular trafficking and export of IL-1β.

Similarly, following 45 min of TcdB stimulation in the presence of 1mM Gd^{3+} or La^{3+} (concentrations that suppress pyroptotic $propidium^{2+}$ influx), WT BMDM also displayed intact ASC oligomerization and caspase-1 activation (Supplemental Fig. 3). Although the presence of 1mM Gd^{3+} or La^{3+} did not prevent the formation of processed caspase-1, the

p20 fragment of caspase-1 and pro-caspase-1 were retained in the cell lysate. Taken together these data demonstrate that Gd^{3+} and La^{3+} do not suppress NLRP3 and Pyrin inflammasome activation or caspase-1 activity, but rather inhibit the downstream pyroptotic signaling processes.

Lanthanides reversibly block the caspase-1-dependent pyroptotic pores and suppress pyroptosis

Given that Gd^{3+} and La^{3+} inhibit caspase-1-dependent PM permeabilization without limiting inflammasome activation, we next investigated the mechanism by which lanthanides target this PM permeability change. Because there is a narrow time window between pyroptotic pore opening and subsequent lysis, we first verified that lanthanides suppress pre-lytic pyroptotic propidium^{2+} influx prior to end-stage lysis by stimulating WT BMDM with NG in the presence of glycine plus or minus 1.5mM Gd^{3+} or 1.2mM La^{3+}. 1.5mM Gd^{3+} and 1.2mM La^{3+} almost completely suppressed pyroptotic propidium^{2+} influx in the presence of glycine, similar to the responses in the absence of glycine (Fig. 6A, B). Interestingly, the lanthanides were more potent as suppressors of pyroptosis-induced propidium^{2+} influx in the presence of glycine than in its absence (Supplemental Fig 3A–D). For example, 800μM Gd^{3+} and La^{3+} partially suppressed the rate and magnitude of NG-induced propidium^{2+} influx in the presence of glycine, but not in the absence of glycine (Supplemental Fig 3E,F). Also, 1mM Gd^{3+} and La^{3+} were more efficacious in reducing the rate and magnitude of NG-induced propidium^{2+} influx in the presence of glycine versus in its absence (Supplemental Fig 3G,H). Together these data indicate that lanthanides target the pre-lytic PM permeability change induced by upstream caspase-1/Gsdmd signaling that may include: 1) gating of large pore channels already resident in the PM or 2) insertion of pore-forming proteins into the PM.

Previous studies have demonstrated that lanthanides can inhibit channels by either acting as competitive pore blockers (55–57) or by binding to anionic phospholipids to induce lateral compression of channels (58, 59). Lanthanides have similar cationic radii as Ca^{2+} enabling them to compete for binding within the selectivity filter of Ca^{2+} channels (55–57). Sukharev and colleagues have reported that Gd^{3+} reversibly inhibits the large mechanosensitive channel (MscL) of *E. coli* by binding to anionic phospholipids (58). Gd^{3+} binding then alters phospholipid packing and greatly increases the lateral pressure within the PM, which forces MscL to adopt a closed conformation (58).

We designed experiments to determine whether the lanthanides reversibly inhibit the pyroptotic pore/channel. After stimulating WT BMDM for 15 min with NG in the presence of propidium^{2+} and 1.5mM Gd^{3+} or 1.2mM La^{3+}, the lanthanide-containing extracellular media was removed and replaced with fresh propidium^{2+} containing media. The removal of Gd^{3+} and La^{3+} rapidly restored the NG-induced propidium^{2+} influx (Fig 6C, D), suggesting that lanthanides reversibly block the Gsdmd-dependent pyroptotic pore/channel.

Next, Gd^{3+}/La^{3+} and propidium^{2+} were added at different times during the course of NLRP3 or Pyrin inflammasome activation to investigate whether lanthanides inhibit the presumed assembly/activation of the pyroptotic pore or the flux of permeant ions through an already assembled/activated pore. When 1.5mM Gd^{3+} or 1.2mM La^{3+} was added to WT BMDM

during NG-induced pyroptotic propidium^{2+} influx (T=20; 20 min post-NG), further dye uptake was prevented (Fig. 6E,F). Similarly, adding 1.5mM Gd^{3+} or La^{3+} to WT BMDM during TcdB-induced pyroptotic propidium^{2+} influx (T=30; 30 min post-TcdB) prevented further dye uptake (Fig. 6G,H). Also, if 1.5mM Gd^{3+} or 1.2mM La^{3+} was added after NG-induced pyroptotic pore opening (20 min post-NG) and propidium^{2+} was added 5 min later (T=20*; propidium^{2+} added 5 min post-lanthanide addition), dye uptake was almost completely suppressed (Fig. 6E,F). Similarly, adding 1.5mM Gd^{3+} or La^{3+} after TcdB-induced pyroptotic pore opening (30 min post-TcdB) and then adding propidium^{2+} 5 min later (T=30*; propidium^{2+} added 5 min post-lanthanide addition) also almost completely suppressed dye uptake (Fig. 6G,H). Residual dye uptake could reflect BMDM that have already progressed to lytic cell death. Because Gd^{3+} and La^{3+} prevented further pyroptotic dye uptake and almost completely prevented any pyroptotic dye uptake if propidium^{2+} was added after Gd^{3+} and La^{3+}, direct pore blockade and/or lateral compression of a pore/channel are plausible mechanisms for how lanthanides reversibly inhibit activity of the pyroptotic pore/channel. Utilizing the lanthanides as a tool to characterize the nature of the caspase-1 dependent PM permeability change suggests that Gd^{3+} and La^{3+} may reversibly inhibit an already active Gsdmd-containing pore or pyroptotic pore/channel(s) regulated by Gsdmd.

Pannexin-1, P2X7R, and certain TRP channel family members are not required for caspase-1-dependent pyroptotic pore induction

Given the observed permeability characteristics and lanthanide sensitivity of the pyroptotic pore/channels, we investigated the potential role of known large-pore channels in mediating caspase-1-dependent pyroptosis. For example, pannexin-1 (Panx1) is an important ATP release channel that adopts a large-pore conformation upon activation and is also permeable to large DNA-intercalating fluorescent dyes (52, 60). Interestingly, Panx1 channels can be gated by apoptotic executioner caspases that excise an autoinhibitory domain from the Panx1 cytosolic C-terminus (60). Núñez and colleagues recently reported that Panx1 is also cleaved by caspase-11 to mediate caspase-11 dependent pyroptosis in macrophages that accumulate cytosolic LPS (47). However, we found that the Panx1 inhibitor trovafloxacin did not suppress NG-induced pyroptotic propidium^{2+} influx in WT BMDM (Fig 7A), suggesting that Panx1 is not required for caspase-1-Gsdmd dependent pre-lytic pore activation in the context of canonical inflammasome-driven pyroptosis.

P2X7R is an ATP-gated non-selective cation channel that can adopt a large-pore conformation that is both permeable to large DNA-intercalating fluorescent dyes and inhibited by Gd^{3+} (52). ATP gating of the P2X7R also mediates NLRP3 inflammasome activation by facilitating K^+ efflux (30, 31, 61). Autocrine activation of P2X7R by ATP released through Panx1 channels has also been implicated in mediating caspase-11 dependent pyroptosis (47). However, we found that the P2X7R antagonists A10606120 and A439079 did not suppress NG-induced propidium^{2+} influx in WT BMDM (Fig 7B). Similarly, *P2rx7*$^{-/-}$ BMDM stimulated with NG or TcdB exhibited comparable rates and magnitudes of propidium^{2+} influx to those observed in WT BMDM (Fig 7C,D). Consistent with this, the absence of P2X7R did not suppress downstream LDH release in response to NG (Fig 7E). These data suggest that the P2X7R is also not required for the caspase-1- and

Gsdmd-dependent pre-lytic pore induction or ensuing pyroptotic lysis downstream of canonical inflammasomes.

We also evaluated the roles of certain members of the TRP channel family, which are non-selective ion channels in mediating caspase-1/Gsdmd-induced pyroptosis given their expression in hematopoietic cells, sensitivity to lanthanides, activation by multiple cell stressors, and roles in innate immunity (51). Specifically, TRPV2 and TRPM7 have been implicated in NLRP3 inflammasome activation in response to hypotonic stress (53). TRPM7 can also be proteolytically gated by apoptotic caspases and is involved in Fas-induced apoptosis (62). TRPM2 is gated in response to oxidative stress (63), and mitochondrial ROS production has been implicated in NLRP3 inflammasome activation (64). In particular, mitochondrial ROS dependent-TRPM2 activation was shown to mediate liposome/particulate induced NLRP3 inflammasome activation (65). We observed that neither the broad TRP channel inhibitor ruthenium red nor the selective TRPM7 inhibitor NS8593 (66, 67) suppressed NG- or TcdB-induced pyroptotic propidium^{2+} uptake (Fig 7F,G). In another recent study (68), we reported that *Trpm2*$^{-/-}$ BMDC stimulated with NG did not exhibit reduced propidium^{2+} influx compared to that in WT cells. Taken together, these experiments indicate that TRPV, TRPM7, or TRPM2 channels are not required components of the caspase-1/Gsdmd-dependent pyroptotic pores.

Discussion

The identity of the caspase-1/11-induced pyroptotic pore/channel(s) remains an elusive component of the pyroptotic cell death signaling cascade. Our findings provide new and mechanistically significant insights regarding the nature of this caspase-1 mediated PM permeability change. We have shown that caspase-1 dependent pyroptosis requires an initial non-lytic permeabilization of the PM that involves the opening of a large, non-selective cation and anion permeable pore/channel(s). Pyroptotic pore activation requires Gsdmd and the activity of the pores can be reversibly inhibited by lanthanides. Furthermore, lanthanide suppression of the caspase-1-and Gsdmd-dependent PM pore/channel has uncovered potential roles for Gsdmd at other intracellular compartments to facilitate pyroptotic cell death and modulate non-classical vesicular trafficking and export of IL-1β.

Recent studies have demonstrated that the cleaved N-terminus of Gsdmd is required for end-stage pyroptotic cell lysis (13, 14, 16). We have shown that Gsdmd is not only necessary for the execution of pyroptotic cell death but is also required for upstream pyroptotic pore induction because pyroptotic propidium^{2+} uptake does not occur in the absence of Gsdmd (Fig. 3C). Possible mechanisms by which cleaved Gdsmd may induce the pyroptotic pore include: 1) Gsdmd forms the pore, 2) Gsdmd functions as a chaperone that enables the effective insertion of the pore into the PM, or 3) Gsdmd directly or indirectly regulates the gating of a pyroptotic channel(s).

Activated caspase-1/11 cleaves cytosolic Gsdmd, which relieves the autoinhibitory interaction between the N and C-terminus such that the N-terminus can execute pyroptotic cell death (13, 14, 16). Necroptosis, a caspase-1/11-independent mode of inflammatory lytic cell death, involves RIP3-mediated phosphorylation of the cytosolic protein mixed lineage

kinase domain-like (MLKL). This drives MLKL oligomerization and insertion into the PM to execute necroptotic cell death (69–71). Phosphorylation of the MLKL C-terminus enables its dissociation from the N-terminal helical protein core, freeing the N-terminus to oligomerize with other MLKL subunits and to insert into the PM to form a death pore (72). This relief of an intramolecular interaction between the C and N-termini of MLKL so that the N-terminus can serve a death executioner function may be analogous to the possible mechanism(s) underlying Gsdmd-mediated cell death. In such a model, cleaved Gsdmd N-terminal fragments may similarly oligomerize and form pyroptotic pores to execute lytic cell death. Future studies are necessary to address whether Gsdmd forms oligomers, localizes to the PM, and can bind membrane lipids. If oligomers of Gsdmd form the pyroptotic pores, it is possible that the pore size could vary under different conditions. Such a scenario might explain the differential rates of propidium^{2+} versus EthD^{4+} dye uptake in response to stimulation with TcdB versus NG (Fig. 2A,B). Another similarity between the PM permeability changes induced by necroptosis and pyroptosis is that La^{3+} also suppresses necroptotic propidium^{2+} accumulation (69). Therefore, lanthanides may function to broadly inhibit large oligomerized protein pores, such as MLKL during necroptotic signaling and, possibly, Gsdmd-containing pores during pyroptotic signaling.

We used the lanthanides Gd^{3+} and La^{3+} as reagents to characterize the caspase-1-Gsdmd dependent change in PM permeability. Gd^{3+} and La^{3+} are known to broadly target large-pore, non-selective cation permeable channels (51, 52). Because lanthanides have similar cationic radii as Ca^{2+}, they competitively block the selectivity filter of Ca^{2+} channels (55–57). Gd^{3+} can reversibly inhibit mechanosensitive bacterial channels (58) by a mechanism that involves binding to anionic phospholipid head groups to exert lateral compression on the channels and thereby result in a closed-pore conformational state (58). We found that millimolar concentrations of lanthanides rapidly and reversibly inhibit the non-lytic, pyroptosis-induced propidium^{2+} influx (Fig. 6A–D). The presence of glycine also enhanced the potency of lanthanides as suppressors of pyroptotic propidium^{2+} uptake (Supplemental Fig.3A–D); this could reflect a selective blocking effect of extracellular lanthanides on activity of the PM pyroptotic pore but not intracellular signaling processes that also contribute to pyroptotic lysis. In the absence of glycine, a higher concentration of Gd^{3+} and La^{3+} is required to effectively inhibit propidium^{2+} influx and corresponding downstream lysis. If pyroptotic propidium^{2+} uptake has already been initiated, La^{3+} and Gd^{3+} act to prevent further dye uptake; lanthanides also completely block influx of dye added after assembly/activation of the PM pore (Fig. 6E–H). Taken together these pharmacologic studies suggest a model of the pyroptotic pore as either an inserted pore-forming protein or a PM resident channel that is gated by accumulation of cleaved Gsdmd. The data further suggest that lanthanides act either to directly block or to laterally compress the pore to a closed conformation upon binding to anionic phospholipid head groups.

Other than functioning as a direct pore-forming protein, Gsdmd may be involved in regulating intrinsic PM proteins that act as pyroptotic pore/channel(s). Núñez and colleagues recently identified P2X7R and Panx1 as important mediators of caspase-11 dependent pyropotosis (47). They showed that intracellular LPS-induced activation of non-canonical inflammasome signaling involved caspase-11-dependent Panx1 cleavage that enabled both K^+ efflux and ATP release (47). K^+ efflux subsequently triggered NLRP3 inflammasome

activation and caspase-1 dependent IL-1β processing and release (47). Autocrine P2X7R activation by the released ATP was required to mediate caspase-11 dependent pyroptosis because LDH release was suppressed in the absence of P2X7R expression or the presence of P2X7R antagonists (47). However, in our model of caspase-1 dependent pyroptosis, the absence of P2X7R, the presence of P2X7R antagonists, or the presence of trovafloxacin (a selective Panx1 inhibitor) did not suppress pyroptotic propidium^{2+} uptake (Fig. 7A–D). Because the absence of P2X7R also did not prevent downstream LDH release (Fig. 7E), these data indicate that neither P2X7R nor Panx1 is an obligatory component of the caspase-1-Gsdmd-mediated pyroptotic cascade. Given that Gsdmd is a substrate of caspase-11 and necessary for caspase-11 mediated pyroptosis (13, 14), future studies should investigate whether Gsdmd regulates Panx1 and/or P2X7R activation as part of the caspase-11 triggered non-canonical inflammasome pathway. Dixit and colleagues demonstrated that caspase-1 activation and processing of IL-1β downstream of non-canonical inflammasome activation depend on Gsdmd (14), suggesting that Gsdmd may regulate or mediate the Panx1-dependent K^+ efflux that drives NLRP3 inflammasome activation secondary to LPS-induced caspase-11 activation.

We investigated TRPM2, TRPV2, and TRPM7 as potential pyroptotic channel candidates due to their known sensitivity to lanthanides and their reported links to NLRP3 inflammasome regulation (53, 65). Additionally, TRPM7 can be proteolytically gated by apoptotic caspases (62). However, we found no critical roles for any of these TRP-family channels in pyroptotic pore function based on either genetic or pharmacologic approaches (Fig. 7F,G). However, TRP channels comprise a large superfamily of non-selective cation channels with 27 members in humans. Therefore, an as-of-yet untested TRP-family channel may be involved in pyroptosis.

Members of the CALHM channel family represent other plausible pyroptotic channel candidates given the known function of CALHM1 as a large pore channel. The CALHM family includes six human homologs. CALHM1 is a voltage-sensitive channel that is responsive to the removal of extracellular calcium and implicated in cortical neuronal excitability (73). It is a non-selective cation- and anion-permeable, large-pore channel with a diameter of 14 angstroms (1.4nm) (74) which is similar to the estimated size range of the pyroptotic pore. It is also sensitive to Gd^{3+} and is an important ATP-release channel that is involved in taste perception (75).

In addition to Gsdmd's role in mediating the permeability change at the PM, our experiments suggest that it may also regulate intracellular functions that contribute to pyroptotic cell lysis. Although lanthanides markedly delayed pyroptotic lysis of WT BMDM and iBMDM, the cells slowly progressed to lytic collapse with prolonged (60 min) NG-stimulated NLRP3 inflammasome signaling despite complete blockade of ionic flux through the PM pore (Supplemental Figs.1and 2). In contrast, *Gsdmd*$^{-/-}$ iBMDM did not exhibit escape from suppression of lytic LDH release during similar prolonged NG stimulation (Fig. 3D). (After >2 h of stimulation, *Gsdmd*$^{-/-}$ iBMDM increasingly progress to apoptosis and then secondary necrosis (Fig. 3E).) This difference between the effects of Gsdmd knockout and lanthanide blockade of the pyroptotic pore on the rate of pyroptotic lysis indicates multiple roles for Gsdmd in integrating pyroptotic signaling downstream of inflammasome

activation. Another member of the *Gsdm* family Gsdma3 has been shown to facilitate mitochondria-dependent cell death (76). Gain of function mutations in the C-terminus of Gsdma3 relieve its autoinhibitory interaction with the N-terminus (76). The N-terminal exposed Gsdma3 is recruited to mitochondria to mediate mitochondrial permeability transition (MPT) and ROS production which disrupts mitochondrial ATP production and drives cell death (76). It is relevant to note that activation of NLRP3 or AIM2 inflammasomes leads to a similar caspase-1-dependent mitochondrial damage (increased ROS production and dissipation of mitochondrial membrane potential) (77). Therefore, cleaved Gsdmd may associate with mitochondria, similar to activated Gsdma3, which disrupts mitochondrial homeostasis and accelerates cell death. Phosphorylated MLKL, which accumulates during the execution of necroptotic lysis, also associates with intracellular organelles, like the mitochondria, lysosome, and ER, in addition to the PM (70). If Gsdmd functions similarly to MLKL, it is possible that cleaved Gsdmd may localize to various organelles to perturb their homeostatic function and thereby modulate progression of pyroptotic cell death.

In contrast to lanthanides, which inhibit the PM pyroptotic pore but not the additional intracellular functions that may contribute to pyroptosis, glycine does not suppress the altered PM permeability to ions and large dyes (Fig. 1,2) but does dramatically delay end-stage lytic pyroptotic cell death. In previous studies of maitotoxin-induced oncotic/necrotic cell death of endothelial cells, glycine was shown to permit non-lytic PM permeability increases to Ca^{2+} and cationic dyes, as well as extensive cell swelling, but to prevent end-stage lysis as assayed through LDH release or GFP loss (41). Because glycine did not suppress the pre-lytic PM permeability to propidium^{2+}, EthD^{4+}, Ca^{2+}, or adenine nucleotides during inflammasome activation (Fig. 1,2), but did prevent LDH release, our data suggest that glycine may preserve the functional integrity of intracellular organelles to greatly delay progression to end-stage pyroptotic lysis. Mootha and colleagues demonstrated that rapidly proliferating cancer cells exhibited a high extent of glycine consumption (78). If enzymes involved in glycine biosynthesis were knocked down, the proliferative capacity of these cancer cells would decrease (78). They also demonstrated that glycine supports a high proliferative capacity of cancer cells by promoting synthesis of purine nucleotides, including ATP (78). During pyroptosis, the caspase-1- and Gdsmd-dependent PM permeabilization will disrupt normal ionic homeostasis and thereby place a large osmotic stress on macrophages. The resulting ionic and osmotic dysregulation will result in enhanced ATP-driven Na^+/K^+ pump activity which, in turn, will place a large metabolic stress on the cell. Future studies should test whether the presence of glycine may sustain ATP synthesis and thereby preserve cellular energetics to delay end-stage pyroptotic cell lysis.

In addition to Gsdmd's role in the execution of pyroptotic cell death, it was also critical for the release of mature caspase-1 and IL-1β into the extracellular environment, but not the intracellular processing of these proteins (Fig. 3E). Shao and colleagues also observed that the absence of Gsdmd prevented IL-1β export without affecting its processing following canonical inflammasome activation (13). Gsdmd may be critical for IL-1β release as a secondary consequence of mediating end-stage pyroptotic lysis; however, our experiments with glycine, which preserves IL-1β and caspase-1 release while suppressing macrophage lysis (Fig. 5), suggest that Gsdmd may additionally regulate non-lytic IL-1β export. Potential

modes of non-lytic release of IL-1β include secretory lysosome exocytosis, microvesicle shedding, multivesicular body formation and fusion with the PM to release exosomes, and autophagy (2, 3). Cookson and colleagues also suggested that direct IL-1β efflux via pyroptotic pores may represent a potential non-lytic release mechanism (19). We tested this possibility by assaying IL-1β and caspase-1 release in the presence of Gd^{3+} and La^{3+}, which block ionic fluxes through the pyroptotic pore. At concentrations that inhibit pyroptotic pore function, lanthanides markedly suppressed the release of mature caspase-1 but not the export of IL-1β (Fig. 5). This suggests that IL-1β and caspase-1 are exported via distinct pathways. In an early investigation of IL-1β and caspase-1 export mechanisms, Kostura and colleagues used electron microscopy of monocytes stimulated with heat-killed *Staphylococcus aureus* to show that immunogold labeled precursor and processed caspase-1 and IL-1β decorated the external surface of the PM (79). This suggested that caspase-1 and IL-1β may associate with PM pores to facilitate their export. Taken together, our comparisons of how Gsdmd-knockout versus the presence of lanthanides or glycine differentially affect IL-1β and caspase-1 export suggest that Gsdmd regulates both non-lytic and lytic mechanisms of release of these inflammatory proteins. In terms of non-lytic export, Gsdmd-dependent pyroptotic pore formation may facilitate caspase-1 and IL-1β permeation through the pore. IL-1β may utilize additional Gsdmd-dependent vesicular trafficking mechanisms because robust IL-1β release is observed during pyroptotic pore inhibition by lanthanides, while the absence of Gsdmd greatly reduces IL-1β export. If cleaved Gsdmd traffics to intracellular organelles, such as mitochondria, to facilitate pyroptotic cell death, analogous to activated Gsdma3 recruitment to mitochondria (76), it is plausible that Gsdmd may also traffic to the recycling endosomal compartments implicated in non-canonical IL-1β release.

In summary, we have characterized the nature of the caspase-1 dependent PM permeability change as a lanthanide-sensitive, Gsdmd-dependent non-selective pore or channel permeable to relatively large organic cations and anions. Gsdmd protein may either comprise the critical subunits of such pores or regulate other proteins that comprise the pyroptotic pores. Gsdmd also facilitates the non-lytic vesicular trafficking and release of IL-1β and may modulate the integrity of intracellular organelles that contribute to the execution of pyroptotic cell death. Whether Gsdmd specifically localizes at the PM and/or other intracellular organelles and how that impacts cellular function and execution of cell death remains to be defined.

Supplementary Material

Refer to Web version on PubMed Central for supplementary material.

Refererences

1. Shi J, Zhao Y, Wang Y, Gao W, Ding J, Li P, Hu L, Shao F. Inflammatory caspases are innate immune receptors for intracellular LPS. Nature. 2014; 514:187–192. [PubMed: 25119034]
2. Carta S, Lavieri R, Rubartelli A. Different Members of the IL-1 Family Come Out in Different Ways: DAMPs vs. Cytokines? Frontiers in immunology. 2013; 4:123. [PubMed: 23745123]
3. Dubyak GR. P2X7 receptor regulation of non-classical secretion from immune effector cells. Cellular microbiology. 2012; 14:1697–1706. [PubMed: 22882764]

4. Gaidt MM, Ebert TS, Chauhan D, Schmidt T, Schmid-Burgk JL, Rapino F, Robertson AA, Cooper MA, Graf T, Hornung V. Human Monocytes Engage an Alternative Inflammasome Pathway. Immunity. 2016; 44:833–846. [PubMed: 27037191]
5. Karmakar M, Katsnelson MA, Dubyak GR, Pearlman E. Neutrophil P2X7 receptors mediate NLRP3 inflammasome-dependent IL-1beta secretion in response to ATP. Nature communications. 2016; 7:10555.
6. Miao EA I, Leaf A, Treuting PM, Mao DP, Dors M, Sarkar A, Warren SE, Wewers MD, Aderem A. Caspase-1-induced pyroptosis is an innate immune effector mechanism against intracellular bacteria. Nature immunology. 2010; 11:1136–1142. [PubMed: 21057511]
7. von Moltke J, Trinidad NJ, Moayeri M, Kintzer AF, Wang SB, van Rooijen N, Brown CR, Krantz BA, Leppla SH, Gronert K, Vance RE. Rapid induction of inflammatory lipid mediators by the inflammasome in vivo. Nature. 2012; 490:107–111. [PubMed: 22902502]
8. Kayagaki N, Warming S, Lamkanfi M, Vande Walle L, Louie S, Dong J, Newton K, Qu Y, Liu J, Heldens S, Zhang J, Lee WP, Roose-Girma M, Dixit VM. Non-canonical inflammasome activation targets caspase-11. Nature. 2011; 479:117–121. [PubMed: 22002608]
9. Kayagaki N, Wong MT, Stowe IB, Ramani SR, Gonzalez LC, Akashi-Takamura S, Miyake K, Zhang J, Lee WP, Muszynski A, Forsberg LS, Carlson RW, Dixit VM. Noncanonical inflammasome activation by intracellular LPS independent of TLR4. Science. 2013; 341:1246–1249. [PubMed: 23887873]
10. Hagar JA, Powell DA, Aachoui Y, Ernst RK, Miao EA. Cytoplasmic LPS activates caspase-11: implications in TLR4-independent endotoxic shock. Science. 2013; 341:1250–1253. [PubMed: 24031018]
11. Doitsh G, Galloway NL, Geng X, Yang Z, Monroe KM, Zepeda O, Hunt PW, Hatano H, Sowinski S, Munoz-Arias I, Greene WC. Cell death by pyroptosis drives CD4 T-cell depletion in HIV-1 infection. Nature. 2014; 505:509–514. [PubMed: 24356306]
12. Franklin BS, Bossaller L, De Nardo D, Ratter JM, Stutz A, Engels G, Brenker C, Nordhoff M, Mirandola SR, Al-Amoudi A, Mangan MS, Zimmer S, Monks BG, Fricke M, Schmidt RE, Espevik T, Jones B, Jarnicki AG, Hansbro PM, Busto P, Marshak-Rothstein A, Hornemann S, Aguzzi A, Kastenmuller W, Latz E. The adaptor ASC has extracellular and 'prionoid' activities that propagate inflammation. Nature immunology. 2014; 15:727–737. [PubMed: 24952505]
13. Shi J, Zhao Y, Wang K, Shi X, Wang Y, Huang H, Zhuang Y, Cai T, Wang F, Shao F. Cleavage of GSDMD by inflammatory caspases determines pyroptotic cell death. Nature. 2015; 526:660–665. [PubMed: 26375003]
14. Kayagaki N I, Stowe B, Lee BL, O'Rourke K, Anderson K, Warming S, Cuellar T, Haley B, Roose-Girma M, Phung QT, Liu PS, Lill JR, Li H, Wu J, Kummerfeld S, Zhang J, Lee WP, Snipas SJ, Salvesen GS, Morris LX, Fitzgerald L, Zhang Y, Bertram EM, Goodnow CC, Dixit VM. Caspase-11 cleaves gasdermin D for non-canonical inflammasome signalling. Nature. 2015; 526:666–671. [PubMed: 26375259]
15. Tamura M, Tanaka S, Fujii T, Aoki A, Komiyama H, Ezawa K, Sumiyama K, Sagai T, Shiroishi T. Members of a novel gene family, Gsdm, are expressed exclusively in the epithelium of the skin and gastrointestinal tract in a highly tissue-specific manner. Genomics. 2007; 89:618–629. [PubMed: 17350798]
16. He WT, Wan H, Hu L, Chen P, Wang X, Huang Z, Yang ZH, Zhong CQ, Han J. Gasdermin D is an executor of pyroptosis and required for interleukin-1beta secretion. Cell research. 2015; 25:1285–1298. [PubMed: 26611636]
17. Broz P, von Moltke J, Jones JW, Vance RE, Monack DM. Differential requirement for Caspase-1 autoproteolysis in pathogen-induced cell death and cytokine processing. Cell host & microbe. 2010; 8:471–483. [PubMed: 21147462]
18. Jorgensen I, Miao EA. Pyroptotic cell death defends against intracellular pathogens. Immunological reviews. 2015; 265:130–142. [PubMed: 25879289]
19. Fink SL, Cookson BT. Caspase-1-dependent pore formation during pyroptosis leads to osmotic lysis of infected host macrophages. Cellular microbiology. 2006; 8:1812–1825. [PubMed: 16824040]

20. Qu Y, Ramachandra L, Mohr S, Franchi L, Harding CV, Nunez G, Dubyak GR. P2X7 receptor-stimulated secretion of MHC class II-containing exosomes requires the ASC/NLRP3 inflammasome but is independent of caspase-1. Journal of immunology. 2009; 182:5052–5062.
21. Li P, Allen H, Banerjee S, Franklin S, Herzog L, Johnston C, McDowell J, Paskind M, Rodman L, Salfeld J, et al. Mice deficient in IL-1 beta-converting enzyme are defective in production of mature IL-1 beta and resistant to endotoxic shock. Cell. 1995; 80:401–411. [PubMed: 7859282]
22. Sanjana NE, Shalem O, Zhang F. Improved vectors and genome-wide libraries for CRISPR screening. Nature methods. 2014; 11:783–784. [PubMed: 25075903]
23. Shalem O, Sanjana NE, Hartenian E, Shi X, Scott DA, Mikkelsen TS, Heckl D, Ebert BL, Root DE, Doench JG, Zhang F. Genome-scale CRISPR-Cas9 knockout screening in human cells. Science. 2014; 343:84–87. [PubMed: 24336571]
24. Antonopoulos C, Russo HM, El Sanadi C, Martin BN, Li X, Kaiser WJ, Mocarski ES, Dubyak GR. Caspase-8 as an Effector and Regulator of NLRP3 Inflammasome Signaling. The Journal of biological chemistry. 2015; 290:20167–20184. [PubMed: 26100631]
25. Katsnelson MA, Rucker LG, Russo HM, Dubyak GR. K+ efflux agonists induce NLRP3 inflammasome activation independently of Ca2+ signaling. Journal of immunology. 2015; 194:3937–3952.
26. Grynkiewicz G, Poenie M, Tsien RY. A new generation of Ca2+ indicators with greatly improved fluorescence properties. The Journal of biological chemistry. 1985; 260:3440–3450. [PubMed: 3838314]
27. Boyd-Tressler A, Penuela S, Laird DW, Dubyak GR. Chemotherapeutic drugs induce ATP release via caspase-gated pannexin-1 channels and a caspase/pannexin-1-independent mechanism. The Journal of biological chemistry. 2014; 289:27246–27263. [PubMed: 25112874]
28. Bergsbaken T, Fink SL, den Hartigh AB, Loomis WP, Cookson BT. Coordinated host responses during pyroptosis: caspase-1-dependent lysosome exocytosis and inflammatory cytokine maturation. Journal of immunology. 2011; 187:2748–2754.
29. Case CL, Kohler LJ, Lima JB, Strowig T, de Zoete MR, Flavell RA, Zamboni DS, Roy CR. Caspase-11 stimulates rapid flagellin-independent pyroptosis in response to Legionella pneumophila. Proceedings of the National Academy of Sciences of the United States of America. 2013; 110:1851–1856. [PubMed: 23307811]
30. Petrilli V, Papin S, Dostert C, Mayor A, Martinon F, Tschopp J. Activation of the NALP3 inflammasome is triggered by low intracellular potassium concentration. Cell death and differentiation. 2007; 14:1583–1589. [PubMed: 17599094]
31. Munoz-Planillo R, Kuffa P, Martinez-Colon G, Smith BL, Rajendiran TM, Nunez G. K(+) efflux is the common trigger of NLRP3 inflammasome activation by bacterial toxins and particulate matter. Immunity. 2013; 38:1142–1153. [PubMed: 23809161]
32. Lyras D, O'Connor JR, Howarth PM, Sambol SP, Carter GP, Phumoonna T, Poon R, Adams V, Vedantam G, Johnson S, Gerding DN, Rood JI. Toxin B is essential for virulence of Clostridium difficile. Nature. 2009; 458:1176–1179. [PubMed: 19252482]
33. Carter GP, Rood JI, Lyras D. The role of toxin A and toxin B in the virulence of Clostridium difficile. Trends in microbiology. 2012; 20:21–29. [PubMed: 22154163]
34. Voth DE, Ballard JD. Clostridium difficile toxins: mechanism of action and role in disease. Clin Microbiol Rev. 2005; 18:247–263. [PubMed: 15831824]
35. Kelly CP, LaMont JT. Clostridium difficile--more difficult than ever. The New England journal of medicine. 2008; 359:1932–1940. [PubMed: 18971494]
36. Xu H, Yang J, Gao W, Li L, Li P, Zhang L, Gong YN, Peng X, Xi JJ, Chen S, Wang F, Shao F. Innate immune sensing of bacterial modifications of Rho GTPases by the Pyrin inflammasome. Nature. 2014; 513:237–241. [PubMed: 24919149]
37. Fink SL, Cookson BT. Pyroptosis and host cell death responses during Salmonella infection. Cellular microbiology. 2007; 9:2562–2570. [PubMed: 17714514]
38. Brennan MA, Cookson BT. Salmonella induces macrophage death by caspase-1-dependent necrosis. Mol Microbiol. 2000; 38:31–40. [PubMed: 11029688]

39. Verhoef PA, Kertesy SB, Estacion M, Schilling WP, Dubyak GR. Maitotoxin induces biphasic interleukin-1beta secretion and membrane blebbing in murine macrophages. Molecular pharmacology. 2004; 66:909–920. [PubMed: 15385641]
40. Verhoef PA, Kertesy SB, Lundberg K, Kahlenberg JM, Dubyak GR. Inhibitory effects of chloride on the activation of caspase-1, IL-1beta secretion, and cytolysis by the P2X7 receptor. Journal of immunology. 2005; 175:7623–7634.
41. Estacion M, Weinberg JS, Sinkins WG, Schilling WP. Blockade of maitotoxin-induced endothelial cell lysis by glycine and L-alanine. American journal of physiology Cell physiology. 2003; 284:C1006–1020. [PubMed: 12477666]
42. Schilling WP, Snyder D, Sinkins WG, Estacion M. Palytoxin-induced cell death cascade in bovine aortic endothelial cells. American journal of physiology Cell physiology. 2006; 291:C657–667. [PubMed: 16672692]
43. Ghiringhelli F, Apetoh L, Tesniere A, Aymeric L, Ma Y, Ortiz C, Vermaelen K, Panaretakis T, Mignot G, Ullrich E, Perfettini JL, Schlemmer F, Tasdemir E, Uhl M, Genin P, Civas A, Ryffel B, Kanellopoulos J, Tschopp J, Andre F, Lidereau R, McLaughlin NM, Haynes NM, Smyth MJ, Kroemer G, Zitvogel L. Activation of the NLRP3 inflammasome in dendritic cells induces IL-1beta-dependent adaptive immunity against tumors. Nature medicine. 2009; 15:1170–1178.
44. Aymeric L, Apetoh L, Ghiringhelli F, Tesniere A, Martins I, Kroemer G, Smyth MJ, Zitvogel L. Tumor cell death and ATP release prime dendritic cells and efficient anticancer immunity. Cancer research. 2010; 70:855–858. [PubMed: 20086177]
45. Arandjelovic S, Ravichandran KS. Phagocytosis of apoptotic cells in homeostasis. Nature immunology. 2015; 16:907–917. [PubMed: 26287597]
46. Lamkanfi M, Kanneganti TD, Van Damme P, Vanden Berghe T, Vanoverberghe I, Vandekerckhove J, Vandenabeele P, Gevaert K, Nunez G. Targeted peptidecentric proteomics reveals caspase-7 as a substrate of the caspase-1 inflammasomes. Mol Cell Proteomics. 2008; 7:2350–2363. [PubMed: 18667412]
47. Yang D, He Y, Munoz-Planillo R, Liu Q, Nunez G. Caspase-11 Requires the Pannexin-1 Channel and the Purinergic P2X7 Pore to Mediate Pyroptosis and Endotoxic Shock. Immunity. 2015; 43:923–932. [PubMed: 26572062]
48. Poon IK, Chiu YH, Armstrong AJ, Kinchen JM, Juncadella IJ, Bayliss DA, Ravichandran KS. Unexpected link between an antibiotic, pannexin channels and apoptosis. Nature. 2014; 507:329–334. [PubMed: 24646995]
49. Chiu YH, Ravichandran KS, Bayliss DA. Intrinsic properties and regulation of Pannexin 1 channel. Channels. 2014; 8:103–109. [PubMed: 24419036]
50. Chekeni FB, Elliott MR, Sandilos JK, Walk SF, Kinchen JM, Lazarowski ER, Armstrong AJ, Penuela S, Laird DW, Salvesen GS, Isakson BE, Bayliss DA, Ravichandran KS. Pannexin 1 channels mediate 'find-me' signal release and membrane permeability during apoptosis. Nature. 2010; 467:863–867. [PubMed: 20944749]
51. Wu LJ, Sweet TB, Clapham DE. International Union of Basic and Clinical Pharmacology. LXXVI. Current progress in the mammalian TRP ion channel family. Pharmacol Rev. 2010; 62:381–404. [PubMed: 20716668]
52. Hansen DB, Ye ZC, Calloe K, Braunstein TH, Hofgaard JP, Ransom BR, Nielsen MS, MacAulay N. Activation, permeability, and inhibition of astrocytic and neuronal large pore (hemi)channels. The Journal of biological chemistry. 2014; 289:26058–26073. [PubMed: 25086040]
53. Compan V, Baroja-Mazo A, Lopez-Castejon G, Gomez AI, Martinez CM, Angosto D, Montero MT, Herranz AS, Bazan E, Reimers D, Mulero V, Pelegrin P. Cell volume regulation modulates NLRP3 inflammasome activation. Immunity. 2012; 37:487–500. [PubMed: 22981536]
54. Lee GS, Subramanian N, Kim AI, Aksentijevich I, Goldbach-Mansky R, Sacks DB, Germain RN, Kastner DL, Chae JJ. The calcium-sensing receptor regulates the NLRP3 inflammasome through Ca2+ and cAMP. Nature. 2012; 492:123–127. [PubMed: 23143333]
55. Lansman JB. Blockade of current through single calcium channels by trivalent lanthanide cations. Effect of ionic radius on the rates of ion entry and exit. The Journal of general physiology. 1990; 95:679–696. [PubMed: 2159974]

56. Mlinar B, Enyeart JJ. Block of current through T-type calcium channels by trivalent metal cations and nickel in neural rat and human cells. The Journal of physiology. 1993; 469:639–652. [PubMed: 8271221]
57. Malasics A, Boda D, Valisko M, Henderson D, Gillespie D. Simulations of calcium channel block by trivalent cations: Gd(3+) competes with permeant ions for the selectivity filter. Biochimica et biophysica acta. 2010; 1798:2013–2021. [PubMed: 20696128]
58. Ermakov YA, Kamaraju K, Sengupta K, Sukharev S. Gadolinium ions block mechanosensitive channels by altering the packing and lateral pressure of anionic lipids. Biophys J. 2010; 98:1018–1027. [PubMed: 20303859]
59. Anishkin A, Loukin SH, Teng J, Kung C. Feeling the hidden mechanical forces in lipid bilayer is an original sense. Proceedings of the National Academy of Sciences of the United States of America. 2014; 111:7898–7905. [PubMed: 24850861]
60. Sandilos JK, Chiu YH, Chekeni FB, Armstrong AJ, Walk SF, Ravichandran KS, Bayliss DA. Pannexin 1, an ATP release channel, is activated by caspase cleavage of its pore-associated C-terminal autoinhibitory region. The Journal of biological chemistry. 2012; 287:11303–11311. [PubMed: 22311983]
61. Sheedy FJ, Grebe A, Rayner KJ, Kalantari P, Ramkhelawon B, Carpenter SB, Becker CE, Ediriweera HN, Mullick AE, Golenbock DT, Stuart LM, Latz E, Fitzgerald KA, Moore KJ. CD36 coordinates NLRP3 inflammasome activation by facilitating intracellular nucleation of soluble ligands into particulate ligands in sterile inflammation. Nature immunology. 2013; 14:812–820. [PubMed: 23812099]
62. Desai BN, Krapivinsky G, Navarro B, Krapivinsky L, Carter BC, Febvay S, Delling M, Penumaka A, Ramsey IS, Manasian Y, Clapham DE. Cleavage of TRPM7 releases the kinase domain from the ion channel and regulates its participation in Fas-induced apoptosis. Developmental cell. 2012; 22:1149–1162. [PubMed: 22698280]
63. Knowles H, Li Y, Perraud AL. The TRPM2 ion channel, an oxidative stress and metabolic sensor regulating innate immunity and inflammation. Immunologic research. 2013; 55:241–248. [PubMed: 22975787]
64. Zhou R, Yazdi AS, Menu P, Tschopp J. A role for mitochondria in NLRP3 inflammasome activation. Nature. 2011; 469:221–225. [PubMed: 21124315]
65. Zhong Z, Zhai Y, Liang S, Mori Y, Han R, Sutterwala FS, Qiao L. TRPM2 links oxidative stress to NLRP3 inflammasome activation. Nature communications. 2013; 4:1611.
66. Chubanov V, Mederos y Schnitzler M, Meissner M, Schafer S, Abstiens K, Hofmann T, Gudermann T. Natural and synthetic modulators of SK (K(ca)2) potassium channels inhibit magnesium-dependent activity of the kinase-coupled cation channel TRPM7. British journal of pharmacology. 2012; 166:1357–1376. [PubMed: 22242975]
67. Chubanov V, Schafer S, Ferioli S, Gudermann T. Natural and Synthetic Modulators of the TRPM7 Channel. Cells. 2014; 3:1089–1101. [PubMed: 25437439]
68. Katsnelson MA, Lozada-Soto KM, Russo HM, Miller BA, Dubyak GR. NLRP3 Inflammasome Signaling is Activated by Low-Level Lysosome Disruption but Inhibited by Extensive Lysosome Disruption: Roles for K+ Efflux and Ca2+ Influx. American journal of physiology. Cell physiology. 2016 ajpcell 00298 02015.
69. Cai Z, Jitkaew S, Zhao J, Chiang HC, Choksi S, Liu J, Ward Y, Wu LG, Liu ZG. Plasma membrane translocation of trimerized MLKL protein is required for TNF-induced necroptosis. Nature cell biology. 2014; 16:55–65. [PubMed: 24316671]
70. Wang H, Sun L, Su L, Rizo J, Liu L, Wang LF, Wang FS, Wang X. Mixed lineage kinase domain-like protein MLKL causes necrotic membrane disruption upon phosphorylation by RIP3. Molecular cell. 2014; 54:133–146. [PubMed: 24703947]
71. Dondelinger Y, Declercq W, Montessuit S, Roelandt R, Goncalves A, Bruggeman I, Hulpiau P, Weber K, Sehon CA, Marquis RW, Bertin J, Gough PJ, Savvides S, Martinou JC, Bertrand MJ, Vandenabeele P. MLKL Compromises Plasma Membrane Integrity by Binding to Phosphatidylinositol Phosphates. Cell reports. 2014; 7:971–981. [PubMed: 24813885]
72. Su L, Quade B, Wang H, Sun L, Wang X, Rizo J. A plug release mechanism for membrane permeation by MLKL. Structure. 2014; 22:1489–1500. [PubMed: 25220470]

73. Ma Z, Siebert AP, Cheung KH, Lee RJ, Johnson B, Cohen AS, Vingtdeux V, Marambaud P, Foskett JK. Calcium homeostasis modulator 1 (CALHM1) is the pore-forming subunit of an ion channel that mediates extracellular Ca2+ regulation of neuronal excitability. Proceedings of the National Academy of Sciences of the United States of America. 2012; 109:E1963–1971. [PubMed: 22711817]

74. Siebert AP, Ma Z, Grevet JD, Demuro A, Parker I, Foskett JK. Structural and functional similarities of calcium homeostasis modulator 1 (CALHM1) ion channel with connexins, pannexins, and innexins. The Journal of biological chemistry. 2013; 288:6140–6153. [PubMed: 23300080]

75. Taruno A, Vingtdeux V, Ohmoto M, Ma Z, Dvoryanchikov G, Li A, Adrien L, Zhao H, Leung S, Abernethy M, Koppel J, Davies P, Civan MM, Chaudhari N, Matsumoto I, Hellekant G, Tordoff MG, Marambaud P, Foskett JK. CALHM1 ion channel mediates purinergic neurotransmission of sweet, bitter and umami tastes. Nature. 2013; 495:223–226. [PubMed: 23467090]

76. Lin PH, Lin HY, Kuo CC, Yang LT. N-terminal functional domain of Gasdermin A3 regulates mitochondrial homeostasis via mitochondrial targeting. J Biomed Sci. 2015; 22:44. [PubMed: 26100518]

77. Yu J, Nagasu H, Murakami T, Hoang H, Broderick L, Hoffman HM, Horng T. Inflammasome activation leads to Caspase-1-dependent mitochondrial damage and block of mitophagy. Proceedings of the National Academy of Sciences of the United States of America. 2014; 111:15514–15519. [PubMed: 25313054]

78. Jain M, Nilsson R, Sharma S, Madhusudhan N, Kitami T, Souza AL, Kafri R, Kirschner MW, Clish CB, Mootha VK. Metabolite profiling identifies a key role for glycine in rapid cancer cell proliferation. Science. 2012; 336:1040–1044. [PubMed: 22628656]

79. Singer II, Scott S, Chin J, Bayne EK, Limjuco G, Weidner J, Miller DK, Chapman K, Kostura MJ. The interleukin-1 beta-converting enzyme (ICE) is localized on the external cell surface membranes and in the cytoplasmic ground substance of human monocytes by immuno-electron microscopy. The Journal of experimental medicine. 1995; 182:1447–1459. [PubMed: 7595215]

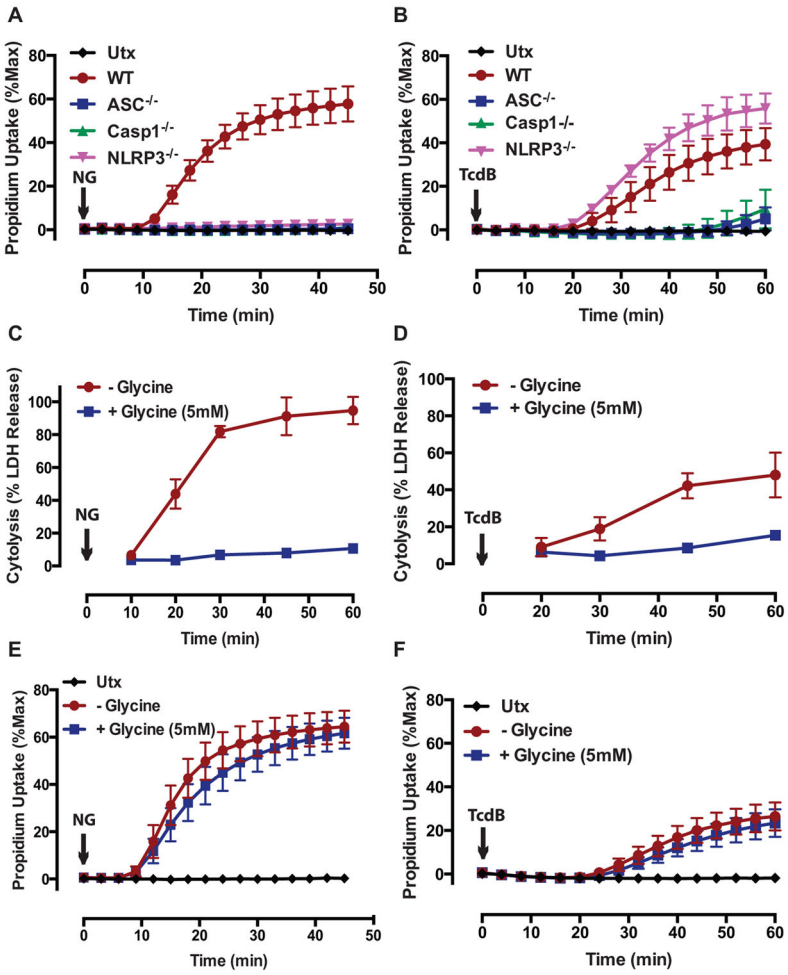

FIGURE 1. A rapidly induced propidium influx is triggered downstream of inflammasome activation but upstream of pyroptotic cell lysis

(A) WT, ASC$^{-/-}$, *Casp1*$^{-/-}$, and NLRP3$^{-/-}$ bone marrow-derived macrophages (BMDM) were primed with LPS (1μg/mL) for 4 h prior to stimulation with nigericin (NG: 10μM) for 45 min, and the change in plasma membrane permeability to propidium^{2+} (1μg/mL) and subsequent accumulation of fluorescent propidium^{2+} (MW: 416Da) complexed with DNA was quantified every 3 min. A 5 min baseline fluorescent read was performed prior to stimulation, and propidium^{2+} fluorescence was expressed as a percentage of maximum fluorescence after adding digitonin (50μg/mL). These data represent the mean ± SE of 6–12 replicates from 4 (WT) or 2 (ASC$^{-/-}$, *Casp1*$^{-/-}$, and NLRP3$^{-/-}$) independent experiments. **(B)** LPS-primed WT, ASC$^{-/-}$, *Casp1*$^{-/-}$, and NLRP3$^{-/-}$ BMDM were stimulated with *C. difficile* toxin B (TcdB: 0.4μg/mL) for 60 min, and propidium^{2+} fluorescence was quantified every 4 min as described in (A). These data represent the mean ± SE of 3–9 replicates from 3 (WT), 2 (ASC$^{-/-}$ and *Casp1*$^{-/-}$), or 1 (NLRP3$^{-/-}$) independent experiments. **(C)** LPS-primed WT BMDM were stimulated with NG or **(D)** TcdB in the presence or absence of the cytoprotectant glycine (5mM). At the indicated times, supernatants were assayed for lactate dehydrogenase (LDH) activity, which was used as an indicator of lytic LDH release. The absorbance values were expressed as a percentage of maximum absorbance following triton

X-100 induced permeabilization of unstimulated LPS-primed cells. These data represent the mean ± SE of 4 replicates from 2 independent experiments. **(E)** LPS-primed WT BMDM were stimulated with NG for 45 min or **(F)** TcdB for 60 min in the presence or absence of 5mM glycine, and propidium^{2+} fluorescence was quantified every 3 or 4 min, respectively. These data represent the mean ± SE of 6 replicates from 2 independent experiments.

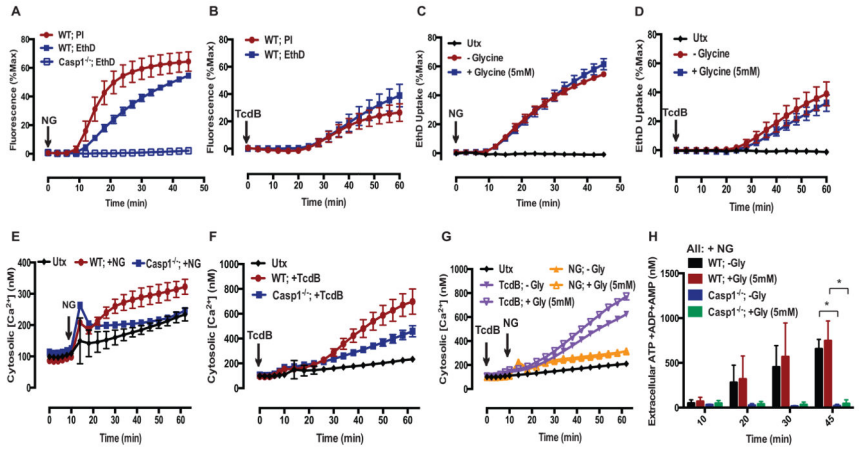

FIGURE 2. NLRP3 and Pyrin inflammasome activation licenses the opening of a large, non-selective cation and anion permeable pyroptotic pore

(A) LPS-primed WT and *Casp1*$^{-/-}$ BMDM were stimulated with NG (10μM) for 45 min, and propidium^{2+} (MW: 416Da) and Ethidium homodimer^{4+} (EthD^{4+}; MW: 788Da, 2μM) fluorescence was quantified every 3 min as described in Fig. 1. These data represent the mean ± SE of 5–6 replicates from 2 independent experiments. **(B)** LPS-primed WT BMDM were stimulated with TcdB (0.4μg/mL) for 60 min, and propidium^{2+} and EthD^{4+} fluorescence was quantified every 4 min. These data represent the mean ± SE of 6 replicates from 2 independent experiments. **(C)** LPS-primed WT BMDM were stimulated with NG for 45 min or **(D)** TcdB for 60 min in the presence or absence of 5mM glycine, and EthD^{4+} fluorescence was quantified every 3 or 4 min, respectively. These data represent the mean ± SE of 5–6 replicates from 2 independent experiments. **(E)** LPS-primed WT and *Casp1*$^{-/-}$ BMDM were stimulated with NG or **(F)** TcdB for 60 min, and the change in cytosolic [Ca^{2+}] was determined using the fluo-4-AM (1μM) Ca^{2+} indicator dye. A 10 min baseline read was taken prior to stimulation. These data represent the mean ± SE of 6 replicates from 2 independent experiments. **(G)** LPS-primed WT and *Casp1*$^{-/-}$ BMDM were stimulated with NG and TcdB in the presence or absence of 5mM glycine for 60 min, and the cytosolic [Ca^{2+}] was determined as described in (E,F). These data represent the mean ± SE of 3–4 replicates from 2 independent experiments. **(H)** LPS-primed WT and *Casp1*$^{-/-}$ BMDM were stimulated with NG in the presence or absence of 5mM glycine. At the indicated times, supernatants were assayed for extracellular [adenine nucleotide] by first rephosphorylating ATP metabolites to ATP and then using a luciferase-based assay to quantify extracellular [ATP]. These data represent the mean ± SE of 4 replicates from 2 independent experiments. *, $p<0.05$.

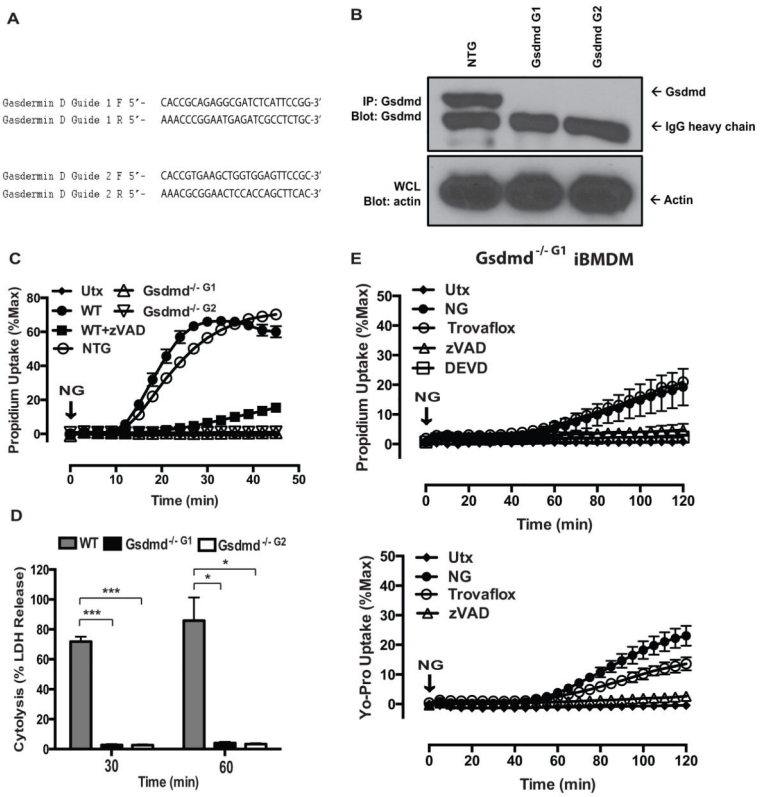

FIGURE 3. Gasdermin D is required for caspase-1 induction of both the pre-lytic pyroptotic pores and subsequent pyroptotic lysis

(A) The guide RNAs used to generate CRISPR-Cas9 *Gsdmd*$^{-/-}$ iBMDM. **(B)** Gsdmd was immunoprecipitated from untreated WT non-targeting guide (NTG), *Gsdmd*$^{-/-}$ Guide 1 (G1: 4 pooled clones), and *Gsdmd*$^{-/-}$ Guide 2 (G2: 2 pooled clones) iBMDM whole cell lysates were incubated overnight with anti-GSDMDC-1 and then with protein-G sepharose. Immunoprecipitated samples were probed for Gsdmd and IgG heavy chain, and soluble cell lysates were probed for actin. These data are representative of results from 1 experiment. **(C)** LPS-primed WT iBMDM in the presence or absence of 50μM zVAD and LPS-primed NTG, *Gsdmd*$^{-/-}$ Guide 1 (*Gsdmd*$^{-/-\ G1}$) and *Gsdmd*$^{-/-}$ Guide 2 (*Gsdmd*$^{-/-\ G2}$) were stimulated with NG (10μM) for 45 min, and propidium^{2+} fluorescence was quantified every 3 min as described in Fig. 1. These data represent the mean ± SE of 4 replicates from 2 independent experiments. **(D)** LPS-primed WT, *Gsdmd*$^{-/-\ G1}$, and *Gsdmd*$^{-/-\ G2}$ iBMDM were stimulated with NG for 30 and 60 min, and the supernatants were subsequently assayed for LDH activity as described in Fig. 1. These data represent the mean ± SE of 4 replicates from 2 independent experiments. ***, $p<0.001$. *, $p<0.05$. **(E)** *Gsdmd*$^{-/-\ G1}$ and *Gsdmd*$^{-/-\ G2}$ iBMDM were stimulated with NG (10μM) for 2 or 3 h, and propidium^{2+} or YoPro^{2+} fluorescence was quantified every 3 min as described in Fig. 1. Where indicated, the assay medium was supplemented with 50 μM zVAD-fmk, 50 μM zDEVD-fmk, or 30 μM trovafloxacin. These data represent the mean ± SE of 4 replicates from 2 independent experiments.

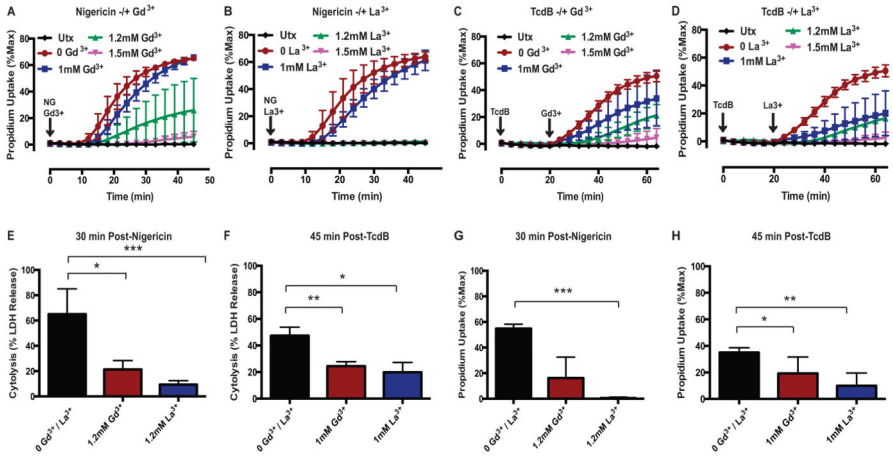

FIGURE 4. Lanthanides coordinately suppress both the caspase-1-dependent plasma membrane permeability change and pyroptotic lysis induced by NLRP3 and Pyrin inflammasome activation

(A) LPS-primed WT BMDM were stimulated with NG (10μM) in the presence or absence of Gd^{3+} (1, 1.2, and 1.5mM) or **(B)** La^{3+} (1, 1.2, 1.5mM) for 45 min, and propidium^{2+} fluorescence was quantified every 3 min as described in Fig. 1. These data represent the mean ± SE of 4 replicates from 2 independent experiments. **(C)** LPS-primed WT BMDM were stimulated with TcdB (0.4μg/mL) in the presence or absence of Gd^{3+} (1, 1.2, and 1.5mM) or **(D)** La^{3+} (1, 1.2, 1.5mM) for 60 min, and propidium^{2+} fluorescence was quantified every 4 min. Gd^{3+} and La^{3+} were added 20 min after TcdB (after the toxin has been internalized but prior to pyroptotic propidium^{2+} influx). These data represent the mean ± SE of 2–8 replicates from 6 independent experiments. **(E)** LPS-primed WT BMDM were stimulated with NG for 30 min in the presence or absence of 1.2mM Gd^{3+} or La^{3+}, and the supernatants were subsequently assayed for LDH activity as described in Fig. 1. These data represent the mean ± SE of 4 replicates from 2 independent experiments. **(F)** LPS-primed WT BMDM were stimulated with TcdB for 45 min in the presence or absence of 1mM Gd^{3+} or La^{3+}, and the supernatants were subsequently assayed for LDH activity. Gd^{3+} and La^{3+} were added 20 min after TcdB. These data represent the mean ± SE of 4 replicates from 2 independent experiments. **(G)** LPS-primed WT BMDM were stimulated as in (E). Propidium^{2+} fluorescence was quantified 30 min post-NG. These data represent the mean ± SE of 4 replicates from 2 independent experiments. **(H)** LPS-primed WT BMDM were stimulated as in (F). Propidium^{2+} fluorescence was quantified 45 min post-TcdB. These data represent the mean ± SE of 8 replicates from 6 independent experiments. *, $p<0.05$. **, $p<0.01$. ***, $p<0.001$.

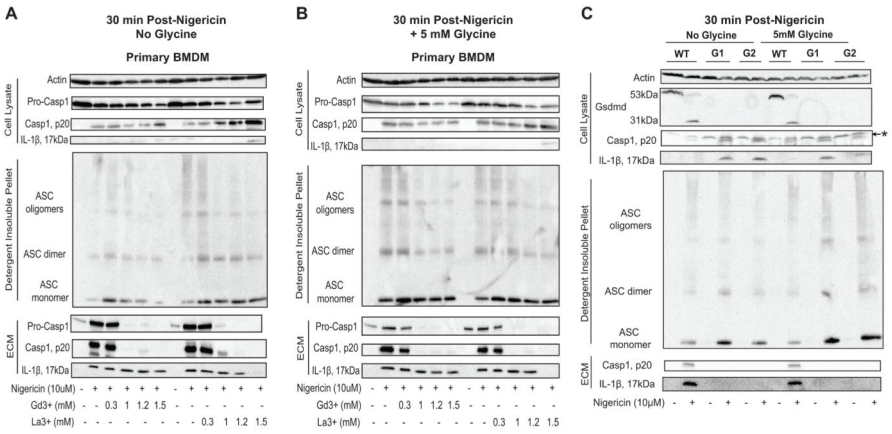

FIGURE 5. Lanthanides do not block NLRP3 inflammasome activation or IL-1β release while Gsdmd deficiency also does not block NLRP3 inflammasome activation but does block IL-1β release

(A) LPS-primed WT BMDM were stimulated with NG (10μM) for 30 min in the presence or absence of Gd^{3+} or La^{3+} (0.3, 1, 1.2, and 1.5mM). The ECM and soluble cell lysates were processed and analyzed on western blot for the presence of caspase-1 and IL-1β. The detergent insoluble fraction was DSS crosslinked and analyzed on western blot for the presence of oligomerized ASC. Western blot analysis of the soluble lysate for actin was also performed. These data are representative of results from 2 experiments. **(B)** LPS-primed WT BMDM were treated as in (A) in the presence of 5mM glycine. The ECM, soluble lysate, and detergent insoluble fraction were analyzed on western blot as described in (A). These data are representative of results from 2 separate experiments. **(C)** LPS-primed WT, *Gsdmd*$^{-/-\,G1}$ (G1), and *Gsdmd*$^{-/-\,G2}$ (G2) iBMDM were stimulated with NG for 30 min. The extracellular media (ECM) and soluble lysates were processed and analyzed on western blot for the presence of caspase-1 and IL-1β. Western blot analysis of the soluble lysate for Gsdmd and actin were also performed. The detergent insoluble fraction of the cell lysates were incubated with the chemical cross-linker disuccinimidyl suberate (DSS) and analyzed on western blot for the presence of ASC monomers, dimers, and oligomers. These data are representative of results from 2 experiments. *: non-specific band .

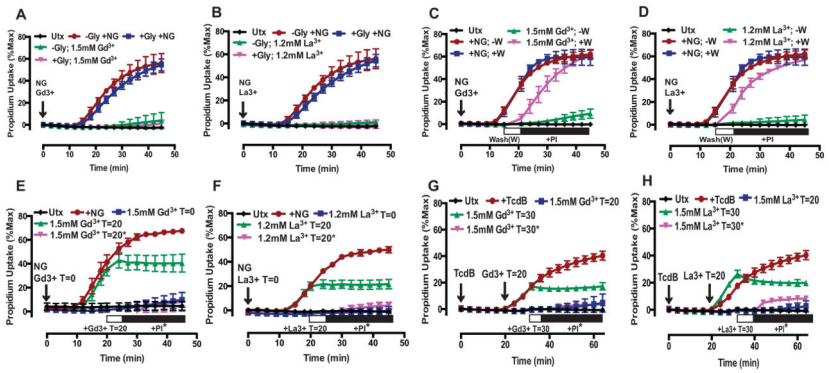

FIGURE 6. Lanthanides reversibly block the caspase-1-dependent pyroptotic pores and suppress pyroptosis

(A) LPS-primed WT BMDM were stimulated with NG (10μM) in the presence or absence of 5mM glycine and +/− 1.5mM Gd^{3+} or **(B)** 1.2mM La^{3+} for 45 min, and propidium^{2+} fluorescence was quantified every 3 min as described in Fig. 1. These data represent the mean ± SE of 4–6 replicates from 2–3 independent experiments. **(C)** LPS-primed WT BMDM were stimulated with NG in the presence or absence of 1.5mM Gd^{3+} or **(D)** 1.2mM La^{3+} for 45 min. At 15 min post-NG stimulation, wells containing WT BMDM, propidium^{2+}, NG, and Gd^{3+}/La^{3+} were either washed with PBS (+W) and replaced with fresh NaCl balanced salt solution (BSS) plus 1μg/mL of propidium^{2+} or not washed (−W). Propidium^{2+} fluorescence was quantified every 3 min. These data represent the mean ± SE of 4–6 replicates from 2–3 independent experiments. **(E)** LPS-primed WT BMDM were stimulated with NG in the presence or absence of 1.5mM Gd^{3+} or **(F)** 1.2mM La^{3+} for 45 min. Propidium^{2+} and lanthanides (Gd^{3+} or La^{3+}) were added at different times during NLRP3 inflammasome activation, which included 1) propidium^{2+} and lanthanides added at the same time as NG (T=0; blue curve), 2) propidium^{2+} added at the same time as NG, and lanthanides added 20 min post-NG (T=20; green curve), or 3) lanthanides added 20 min post-NG, and propidium^{2+} added 5 min post-lanthanide addition (T=20*; magenta curve). Propidium^{2+} fluorescence was quantified every 3 min. These data represent the mean ± SE of 4–6 replicates from 3 (E) or 2 (F) separate experiments. **(G)** LPS-primed WT BMDM were stimulated with TcdB in the presence or absence of 1.5mM Gd^{3+} or **(H)** La^{3+} for 60 min. Propidium^{2+} and lanthanides were added at different times during Pyrin inflammasome activation, which included 1) propidium^{2+} added at the same time as TcdB, and lanthanides added 20 min post-TcdB (T=20; blue curve), 2) propidium^{2+} added at the same time as TcdB, and lanthanides added 30 min post-TcdB (T=30; green curve), or 3) lanthanides added 30 min post-TcdB, and propidium^{2+} added 5 min post-lanthanide addition (T=30*; magenta curve). Propidium^{2+} fluorescence was quantified every 4 min. These data represent the mean ± SE of 2–8 replicates from 2 independent experiments.

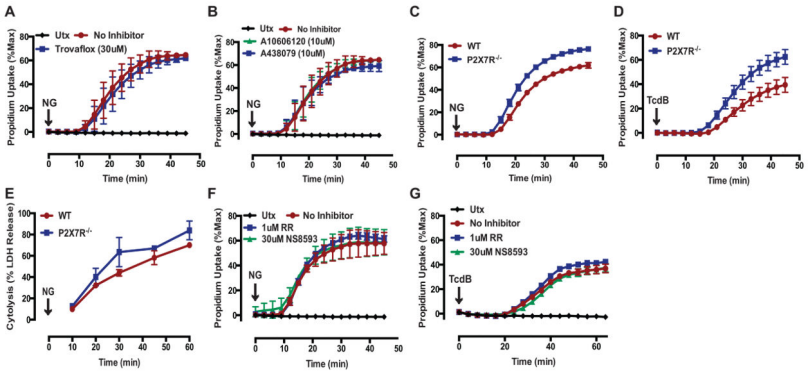

FIGURE 7. Pannexin-1, P2X7R, and certain TRP channel family members are not required for caspase-1-dependent pyroptotic pore induction

(A) LPS-primed WT BMDM were stimulated with NG (10μM) for 45 min in the presence or absence of the pannexin 1 inhibitor trovafloxacin (30μM). These data represent the mean ± SE of 4 replicates from 2 independent experiments. **(B)** LPS-primed WT BMDM were stimulated with NG for 45 min in the presence of the P2X7R antagonists A10606120 (10μM) or A438079 (10μM). These data represent the mean ± SE of 4 replicates from 2 independent experiments. **(C)** LPS-primed WT or P2X7R$^{-/-}$ BMDM were stimulated with NG or **(D)** TcdB (0.4μg/mL) for 45 min. These data represent the mean ± SE of 3 replicates from 1 experiment. **(A–D)** Propidium^{2+} fluorescence was quantified every 3 (NG) or 4 (TcdB) min as described in Fig. 1. **(E)** LPS-primed WT or P2X7R$^{-/-}$ BMDM were stimulated with NG. At the indicated times, supernatants were assayed for LDH activity as described in Fig. 1. These data represent the mean ± SE of 2 replicates from 1 experiment. **(F)** LPS-primed WT BMDM were stimulated with NG for 45 min or **(G)** TcdB for 60 min in the presence of the TRPV channel inhibitor ruthenium red (RR: 1μM) or the TRPM7 channel inhibitor NS8593 (30μM). These data represent the mean ± SE of 2–4 replicates from 2 (F) or 1 (G) independent experiments. **(F–G)** Propidium^{2+} fluorescence was quantified every 3 (NG) or 4 (TcdB) min as described in Fig. 1.